European Journal of Medicinal Chemistry 141 (2017) 373–385

Contents lists available at ScienceDirect

European Journal of Medicinal Chemistry

journal homepage: http://www.elsevier.com/locate/ejmech

Research paper

# Discovery of novel anti-angiogenesis agents. Part 8: Diaryl thiourea bearing 1*H*-indazole-3-amine as multi-target RTKs inhibitors

Ying Sun [a, 1], Yuanyuan Shan [b, 1], Chuansheng Li [a], Ru Si [a], Xiaoyan Pan [a], Binghe Wang [c], Jie Zhang [a, *]

[a] School of Pharmacy, Health Science Center, Xi'an Jiaotong University, No. 76, Yanta West Road, Xi'an, 710061, China
[b] Department of Pharmacy, The First Affiliated Hospital of Xi'an Jiaotong University, Xi'an, 710061, China
[c] Department of Chemistry and Center for Diagnostics and Therapeutics, Georgia State University, Atlanta, GA, 30303, United States

ARTICLE INFO

*Article history:*
Received 25 June 2017
Received in revised form
30 September 2017
Accepted 3 October 2017
Available online 6 October 2017

*Keywords:*
Anti-angiogenesis agents
Multi-target
RTK inhibitors
Hinge-binding group
1*H*-indazol-3-amine

ABSTRACT

VEGFR-2, TIE-2, and EphB4 are essential for both angiogenesis and tumorigenesis. Herein, we designed and prepared three classes of multi-target inhibitors based on the extensive sequence homology along the kinase domain of angiogenic RTKs. Biological evaluation indicated that these multi-target inhibitors exhibited considerable potential as novel anti-angiogeneic and anticancer agents. Among them, a diaryl thiourea bearing 1*H*-indazole-3-amine (16a) displayed the most potent RTK inhibition and excellent selectivity. It also showed inhibition on viability of human umbilical vein endothelial cells and anti-proliferation against a broad spectrum of cancer cells. Therefore, 1*H*-indazole-3-amine could serve as a promising hinge binding group for multi-target inhibitors of VEGFR-2, Tie-2, and EphB4.

© 2017 Elsevier Masson SAS. All rights reserved.

## 1. Introduction

Dr. Folkman's dedication to understanding the role of angiogenesis in disease has given rise to novel therapies for various diseases including cancer, inflammatory, and vision-threatening diseases [1]. Angiogenesis is a complex process and tightly modulated by a multitude of pro- and anti-angiogenic factors [2]. Pathological angiogenesis can be activated by activation of various pro-angiogenic factors. In the past decades, numbers of pro-angiogenic factors such as VEGFR-2, Tie-2, and EphB4 have been identified as potential targets for angiogenesis inhibitors [3]. Anti-angiogenesis agents have been considered as a valid strategy for the treatment of cancers [4]. Angiogenesis is tightly controlled by the equilibrium between pro- and anti-angiogenic factors which are expressed on endothelial cells (ECs). VEGFR-2 mainly contributed to very early steps of angiogenesis. Meanwhile, Tie-2 and EphB4 contributed to later steps of angiogenesis [5]. Recently, mounting evidence indicates that tumors become refractory or even bypass the inhibition of a single pro-angiogenic factor via compensatory activation of alternative pro-angiogenic factors [6]. The understandings of compensatory activation and cross-talk for sustaining angiogenesis is essential and may act as a basic prerequisite for designing multi-target RTK inhibitors as anti-angiogenic agents [7].

To the best of our knowledge, the majority of RTKs contain a highly conserved catalytic ATP binding site. Sequence comparison of the three RTKs in question indicated extensive sequence homology along the kinase domain (Fig. 1) [8,9]. We believe that the sequence homology and structural similarity of the three RTKs make it feasible to design multiplex inhibitors.

We are interested in the discovery of novel anti-angiogenesis agents. Along this line, structural optimization of natural alkaloid taspine afforded many biphenyl derivatives as novel VEGFR-2 inhibitors [10–13]. Several diaryl ureas bearing a salicylaldoxime including BPS-7 have been identified as potent VEGFR-2 inhibitors (Fig. 2) [14–16]. Very importantly, BPS-7 displayed potent inhibition against angiogenic EphB4 and Tie-2. It also significantly inhibited the proliferation of human umbilical vein endothelial cells (HUVECs) [17]. In addition, BPS-7 effectively inhibited blood vessel formation in a tissue model for angiogenesis. These findings encouraged us to develop novel triple inhibitors of VEGFR-2/TIE-2/EphB4 as anti-angiogenic and anticancer agents.

* Corresponding author.
*E-mail address:* zhj8623@xjtu.edu.cn (J. Zhang).
[1] Both authors contributed equally to this work and should be regarded as joint first authors.

https://doi.org/10.1016/j.ejmech.2017.10.008
0223-5234/© 2017 Elsevier Masson SAS. All rights reserved.

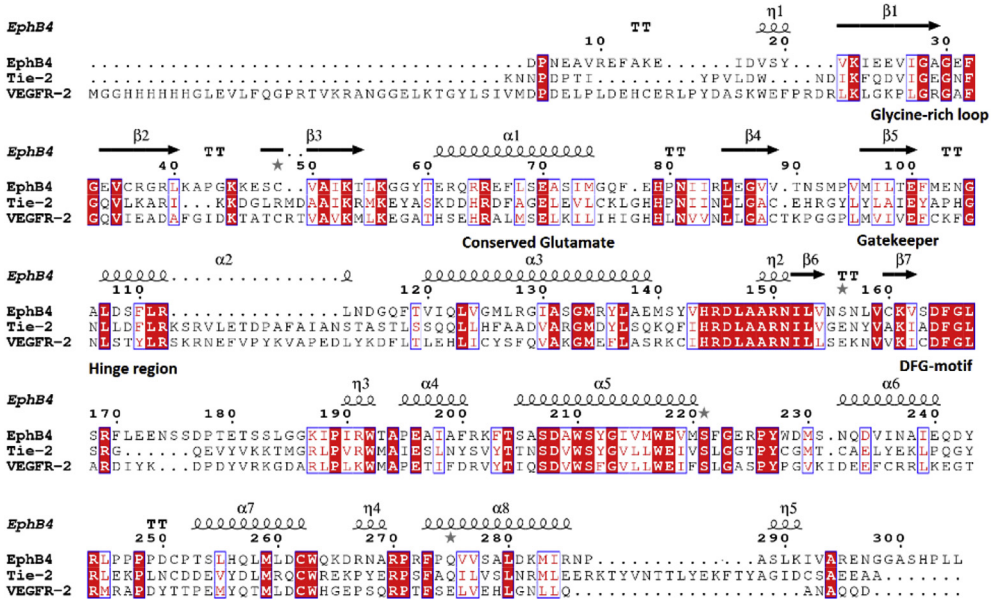


**Fig. 1.** Sequence alignment of ATP-binding pocket of the three RTKs: VEGFR-2 (PDB ID: 4ASD), Tie-2 (PDB ID: 2P4I), and EphB4 (PDB ID: 2X9F) using Cobalt. Secondary structures were represented with EphB4 crystal structure using ENDscript server.

Based on the high sequence homology of three RTKs (VEGFR-2/Tie-2/EphB4) and similar pharmacophore of their inhibitors, we propose that the rational design of multi-target inhibitors of VEGFR-2/Tie-2/EphB4 is a promising strategy for the discovery of anti-angiogenic agents. Previously, BPS-7 was identified as privileged scaffold of VEGFR-2 inhibitor. Our continuous efforts focused on the development of novel anti-angiogenic agents based on the binding mode of BPS-7 with RTKs. In doing so, structural optimization of BPS-7 have been dissected into four regions (Fig. 3). First, we explored various heteroaromatics as hinge binding group (HBG) via core-refining approach. Pyridin-2-amine, *N*-(pyridin-2-yl)acryl amide, 1*H*-indazol-3-amine, and quinazolin-4(3*H*)-one were introduced as new HBG. We reasoned that it is possible that these groups could form hydrogen bonds with RTKs and therefore provide an opportunity to improve affinity. Second, the two methoxyl groups on scaffold of BPS-7 were removed to reduce the steric hindrance in binding with the respective receptor. Third, inspired by the classic bioisosteric paradigm, urea was replaced with thiourea which bear hydrogen bond donors and acceptors. Moreover, the urea moiety was replaced with cyclobutane-1,1-dicarboxamide which bear more hydrogen bond donors and acceptors. Fourth, various anilines were incorporated as they are beneficial for antitumor potency and could enhance the persistence [18].

Encouraged by previous results, we proposed that multiple

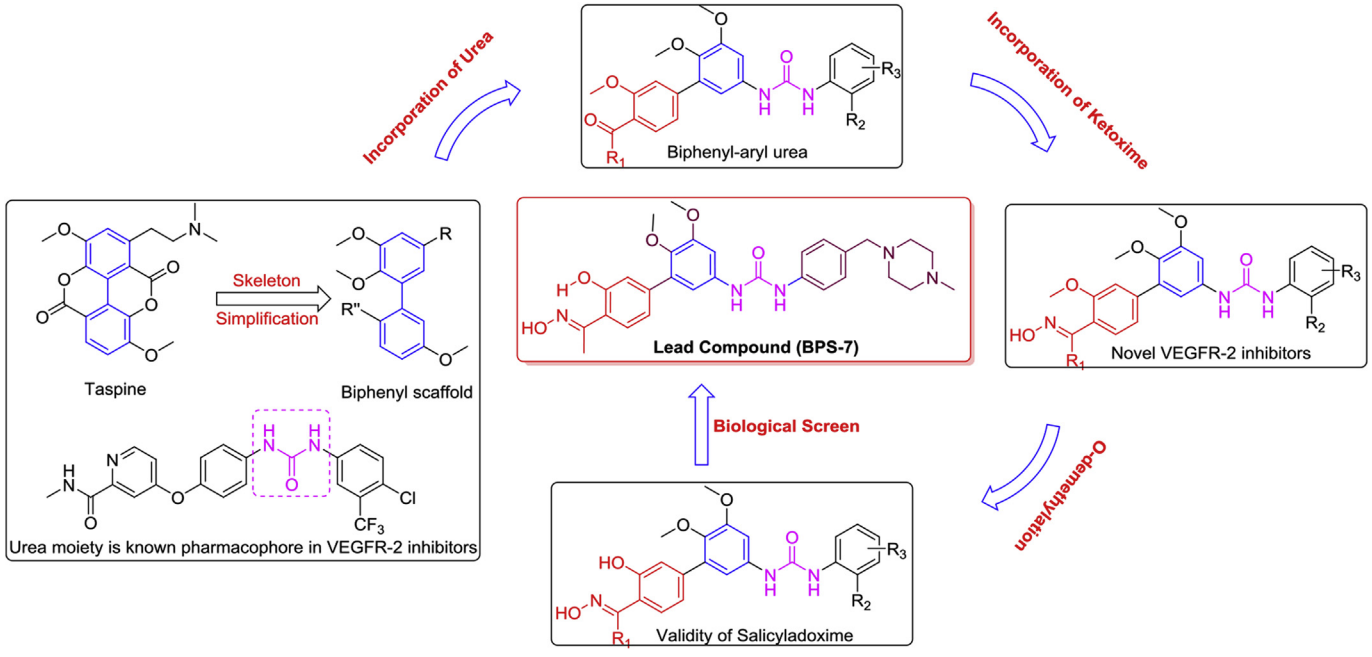


**Fig. 2.** Structural optimization of taspine and discovery of novel multi-target lead compound (**BPS-7**).

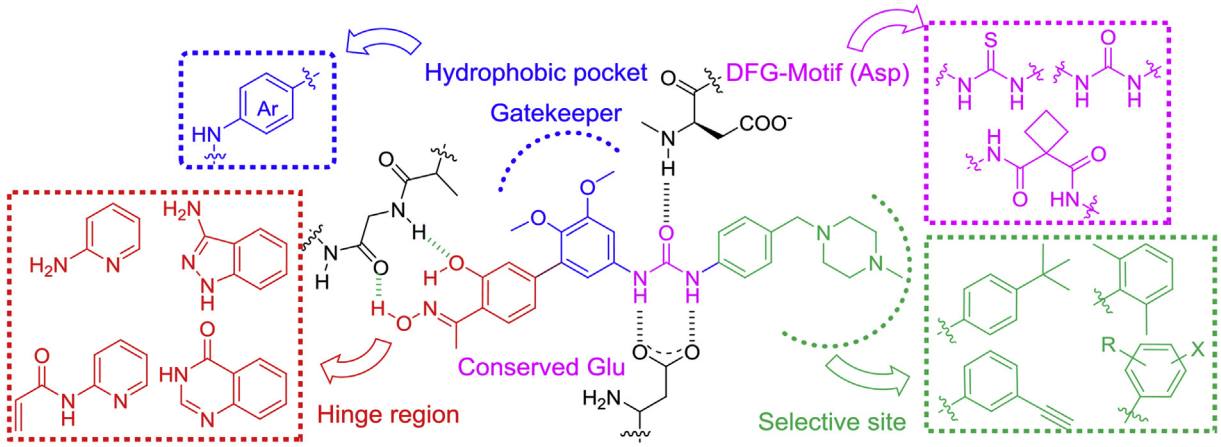


**Fig. 3.** Design strategy and structures of novel multi-target anti-angiogenesis agents derived from BPS-7.

inhibition of RTKs could afford novel anti-angiogenic agents. For this reason, efforts are being initiated to find novel multi-target inhibitors, in order to explore molecular diversities and discovery original pharmacophores and chemotypes. These compounds with 'triplet' inhibition profile have been identified as novel anti-angiogenic and anticancer agents. Several biphenyl-aryl thioureas incorporated with 1*H*-indazol-3-amine exhibited promising anti-angiogenic and anti-cancer potency. The representative compound 16a exhibited prominent anti-angiogenic and anticancer activities and could be considered as a novel lead compound for further optimization.

## 2. Results and discussion

### 2.1. Chemistry

Scheme 1 depicts the synthesis of diaryl thiourea derivatives **16a-16e**. 4-Iodo-1*H*-indazol-3-amine **2** was prepared from 2-fluoro-6-iodobenzonitrile **1** and hydrazine hydrate in the presence of $NaHCO_3$. Subsequently, the key intermediate **4** was prepared through a Suzuki coupling of **2** with 4-aminophenylboronic acid **3**. Various anilines were treated with $CS_2$ to generate **5**, which was treated with bis(trichloromethyl)carbonate (BTC) to yield intermediates **6**. Finally, reaction of isothiocyanates **6** with biphenyls **4** afforded the title compounds **16a-16e**.

The synthetic route for diaryl ureas **17a-17n** was described in Scheme 2. Firstly, various substituted anilines were treated with triphosgene in anhydrous $CH_2Cl_2$ yielding isocyanates. Subsequently, reaction of isocyanates with 4-(4,4,5,5-tetramethyl-1,3,2-dioxaborolan-2-yl)aniline **7** gave diaryl ureas **8**. $Pd(PPh_3)_4$ catalyzed Suzuki coupling of **8** with 2-amino-5-bromopyridine **9** in presence of $K_2CO_3$ in acetonitrile/$H_2O$ afforded the key intermediates **10**. Finally, the title compounds **17a-17n** were prepared through acylation of **10** with acryloyl chloride.

The synthesis of title compounds **18a-18g** was shown in Scheme 3. Firstly, intermediate **13** was prepared from **12** [19] and 4-

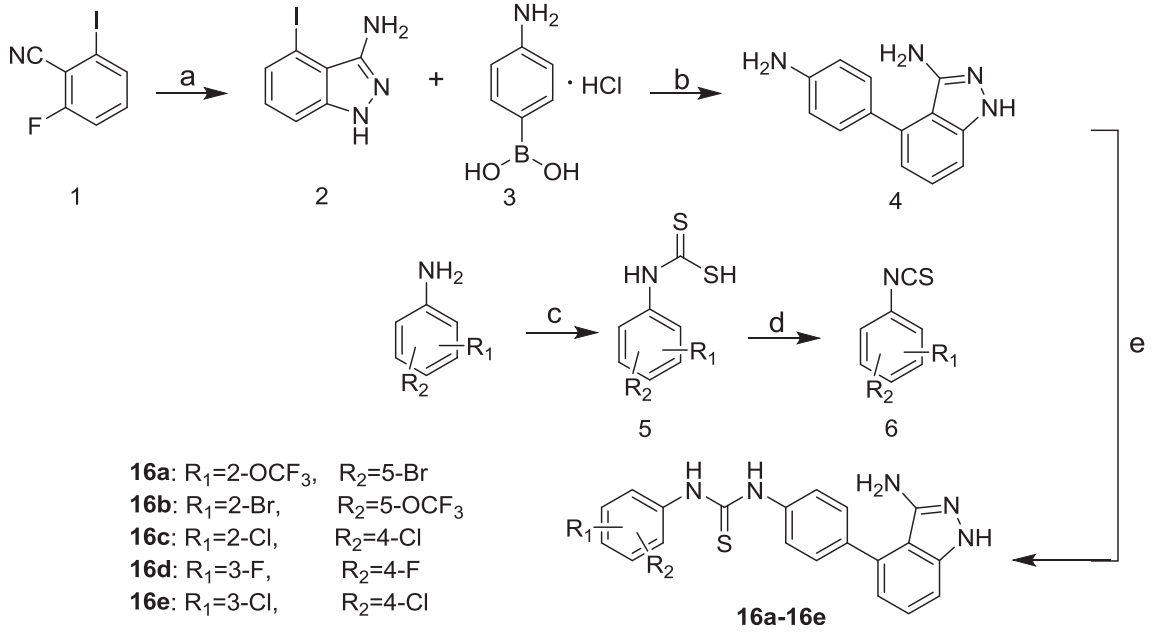


**Scheme 1.** Synthesis of diarylthiourea derivatives 16a-16e.
**Reagents and conditions**: (a) $CH_3CH_2OH$, $NaHCO_3$, $NH_2NH_2$, $H_2O$; (b) $Pd(PPh_3)_4$, $Na_2CO_3$, $H_2O$, dioxane; (c) $CH_2Cl_2$, room temperature; (d) DABCO, $CS_2$, toluene; (e) BTC, $CH_2Cl_2$.

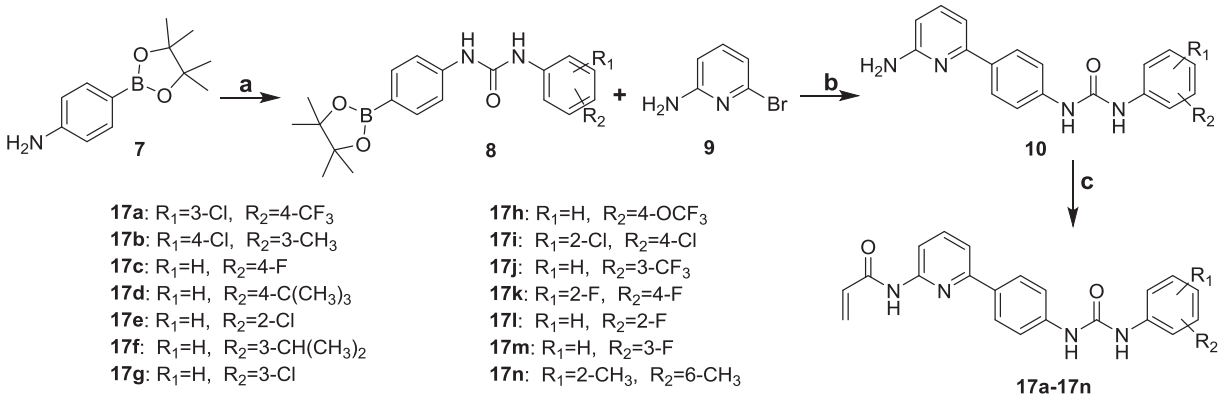


**Scheme 2.** Synthesis of *N*-(pyridin-2-yl)acrylamide diaryl urea derivatives 17a-17n.
**Reagents and conditions**: (a) R-$NH_2$, BTC, $Et_3N$, $CH_2Cl_2$, 0 °C to rt; (b) $Pd(PPh_3)_4$, $K_2CO_3$, $H_2O$, $CH_3CN$, reflux, 100 °C; (c) Acryloyl chloride, $Et_3N$, THF, 0 °C to rt.

aminophenylboronic acid **3** through Pd-catalyzed Suzuki coupling. Condensation of **14** with various substituted anilines in the presence of thionyl chloride gave intermediates **15**. Finally, treatment of intermediates **13** with **15** in the presence of *o*-(7-azabenzotriazol-1-yl)-*N,N,N′,N′*-te-tramethyluronium hexafluorophosphat (HATU) afforded title compounds **18a-18g**.

All the title compounds are characterized by $^1$H NMR, $^{13}$C NMR, high resolution mass spectrum (HRMS), and melting point analysis. The purity of title compound was above 95% which was determined by HPLC analysis (Supplementary Material).

### 2.2. Biology assays

The three targeted RTKs are involved in both angiogenesis and tumorigenesis [20]. With the aim to evaluate the biological activities of title compounds as anti-angiogenic and anticancer agents, we firstly performed the biological evaluation of the title compounds concerning their inhibitory efficacy and selectivity on RTKs. Subsequently, in order to validate the dual function of the title compounds, their inhibition on viability of HUVECs (EA.hy926) was examined in a first screening to prove the anti-angiogenic potency and antiproliferation on a panel of cancer cells was tested to prove the anticancer activity. In parallel, a marketed multi-target RTK inhibitors approved by the FDA, sorafenib, was used as positive control.

#### 2.2.1. In vitro receptor tyrosine kinases inhibition assay

In order to validate the direct effect of title compounds on VEGFR-2, Tie-2, and EphB4 kinase, we performed *in vitro* kinase assay using ADP-Glo Kinase Assay Kit (Promega, Wisconsin, USA). The biological evaluation results were depicted in Tables 1–3 with sorafenib as positive control.

In analyzing the inhibition data, we first look at the implications of the urea core by replacement of urea moiety with thiourea and thus the hinge binding group of BPS-7 [21]. 1*H*-indazol-3-amine were introduced as hinge binding groups. It has been verified that compounds with thiourea were more potent than the ureas. Therefore, further modification focused on thioureas with dihalogen substituted aniline and 1*H*-indazol-3-amine was incorporated as HBG (Table 1). The results showed that all the title compounds exhibited simultaneously inhibitory potency against VEGFR-2, Tie-2, and EphB4 with $IC_{50}$ values less than 50 nM. In particular, 16a was the most potent multi-target RTKs inhibitors with $IC_{50}$ values of 3.45 nM (VEGFR-2), 2.13 nM (Tie-2), and 4.71 nM (EphB4), respectively. The results highlighted the importance of 1*H*-indazol-3-amine for improving the simultaneous inhibition of these multiple inhibitors. This study identified that 1*H*-indazol-3-amine was an excellent hinge binding group for multi-target inhibitors of VEGFR-2, Tie-2, and EphB4.

Inspired by the above investigation, *N*-(pyridin-2-yl)acryl amide was introduced as novel hinge binding group (Table 2). The activity data indicated that three title compounds (17a, 17b, and 17l) exhibited simultaneous and potent inhibition against VEGFR-2, Tie-2, and EphB4. In particular, 17b bearing 4-chlorine-3-trifluoromethyl substituent at terminal aniline was the most potent multi-target RTK inhibitor with $IC_{50}$ values of 6.17 nM (VEGFR-2), 13.75 nM (Tie-2), and 7.23 nM (EphB4), respectively. The results suggested that *N*-(pyridin-2-yl)acryl amide could serve as a hinge binding group for multi-target inhibitors of VEGFR-2, Tie-2, and EphB4.

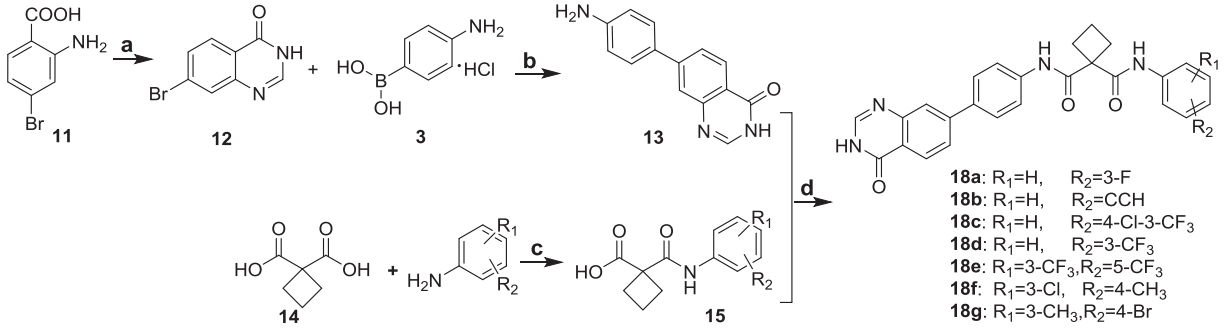


**Scheme 3.** Synthesis of quinazolinone cyclobutanebiamide derivatives 18a-18g.
**Reagents and conditions**: (a) $HCONH_2$, MW, 300W, 150 °C, 1.45h; (b) $Pd(PPh_3)_4$, $K_2CO_3$, $H_2O$, dioxane, reflux, 100 °C; (c) $SOCl_2$, $Et_3N$, $CH_2Cl_2$, 0 °C to rt; (d) HATU, $Et_3N$, THF, 0 °C to rt.

**Table 1**
Structures and RTKs inhibitory activities of title compounds (**16a-16e**) ($IC_{50}$, nM).

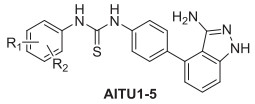


| Compound | $R_1$ | $R_2$ | VEGFR-2 | TIE-2 | EphB4 |
|---|---|---|---|---|---|
| 16a | 2-$OCF_3$ | 5-Br | 3.45 | 2.13 | 4.71 |
| 16b | 2-Br | 5-$OCF_3$ | 7.94 | 4.85 | 12.10 |
| 16c | 2-Cl | 4-Cl | 24.33 | 19.80 | 21.35 |
| 16d | 3-F | 4-F | 19.97 | 28.32 | 15.46 |
| 16e | 3-Cl | 4-Cl | 7.66 | 16.70 | 17.48 |
| Sorafenib | | | 1.27 | 7.85 | 4.62 |

We are enlightened by the above potent multiple inhibitors with new hinge binding group. Subsequently, quinazolin-4(3*H*)-one was incorporated as a novel hinge binding group which afford much benefit to RTK inhibition. In order to better understand the functional group tolerance at the urea core, we investigated cyclobutane-1,1-dicarboxamide in addition to cyclopropane-1,1-dicarboxamide and thiourea yielding compounds (18a-18g) (Table 3). Not surprisingly, these compounds exhibited poor RTKs inhibitory potency compared with diaryl ureas and diaryl thioureas, which revealed that cyclobutane-1,1-dicarboxamide could not serve as the core structure interacting with DFG-motif of RTKs.

### 2.2.2. RTK selectivity assay

In order to determine the RTK selectivity profile of two most potent compounds, 16a, a broad panel kinase screening was further conducted by evaluating the inhibition against other ten RTKs including VEGFR-1, VEGFR-3, EGFR, FGFR-1, FGFR-4, PDGFR-β, IGF1-R, B-Raf, c-Kit, and c-Met (Fig. 4). Besides VEGFR-2, Tie-2, and EphB4, 16a displayed moderate inhibitory activity against FGFR-1 and PDGFR-β. Interestingly, it also exhibited potent inhibition against VEGFR-1, VEGFR-3, and B-Raf with $IC_{50}$ values less than 50 nM. The results confirmed that this multi-target inhibitor exhibited good selectivity on VEGFR-2/TIE-2/EphB4 relative to other RTKs including EGFR, FGFR-1, FGFR-4, IGF1-R, c-Kit, and c-Met.

**Table 3**
Structures and RTKs inhibitory activities of title compounds (**18a-18g**) ($IC_{50}$, nM).

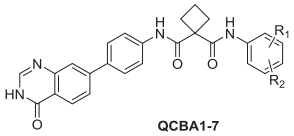


| Compound | $R_1$ | $R_2$ | VEGFR-2 | Tie-2 | EphB4 |
|---|---|---|---|---|---|
| 18a | H | 3-F | >500 | 42.15 | >500 |
| 18b | H | -CCH | >500 | 22.15 | >500 |
| 18c | 4-Cl | 3-$CF_3$ | 297.02 | 88.64 | >500 |
| 18d | H | 3-$CF_3$ | 310.64 | 73.59 | 93.36 |
| 18e | 3-$CF_3$ | 5-$CF_3$ | >500 | 133.47 | 216.58 |
| 18f | 3-Cl | 4-$CH_3$ | 31.40 | 115.15 | >500 |
| 18g | 2-CH3 | 4-Br | >500 | 64.33 | >500 |
| Sorafenib | | | 1.27 | 7.85 | 4.62 |

### 2.2.3. Effects of multi-target inhibitors on the human umbilical vein endothelial cells (HUVECs) viability

In order to determine the potential anti-angiogenic effect of these multi-target inhibitors, we evaluate the inhibition of title compounds on HUVECs (EA.hy926) viability using cell counting kit-8 (CCK-8) method [22]. Highly consistent with their potent RTK inhibitory activity, the majority of title compounds displayed dose-dependent inhibition of EA.hy926 viability with $IC_{50}$ values ranging from 12.63 μM to 225.62 μM (Table 4). Interestingly, four compounds (16a, 16e, 17a, and 18f) exhibited more potent inhibition on viability of HUVECs than others with $IC_{50}$ values less than 20 μM. These results demonstrated that these compounds might display anti-angiogenic potency through decreasing viability of HUVECs (EA.hy926).

### 2.2.4. Anti-proliferative activity against cancer cells

RTKs and angiogenesis played critical role in the proliferation of various cancers cells and RTK inhibition generally translated well into anti-proliferation of cancer cells. In this regard, in order to investigate the potential anticancer potency of these multi-target RTK inhibitors, the most potent 16a was selected to examine its anti-proliferative activity against nine cancer cells including human hepatic cancer cell lines (HepG2, SMMC-7721),

**Table 2**
Structures and RTKs inhibitory activities of title compounds (**17a-17n**) ($IC_{50}$, nM).

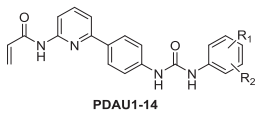


| Compound | $R_1$ | $R_2$ | VEGFR-2 | Tie-2 | EphB4 |
|---|---|---|---|---|---|
| 17a | 4-Cl | 3-$CF_3$ | 6.17 | 13.75 | 7.23 |
| 17b | 3-Cl | 4-$CH_3$ | 7.05 | 14.20 | 7.68 |
| 17c | H | 4-F | >500 | >500 | >500 |
| 17d | H | 4-$C(CH_3)_3$ | 11.90 | 68.68 | 73.43 |
| 17e | H | 2-Cl | >500 | 10.29 | 44.52 |
| 17f | H | 3-$CH(CH_3)_2$ | >500 | 97.74 | 106.84 |
| 17g | H | 3-Cl | 122.81 | 31.15 | >500 |
| 17h | H | 4-$OCF_3$ | >500 | 98.12 | 86.65 |
| 17i | 2-Cl | 4-Cl | >500 | 21.52 | 87.24 |
| 17j | H | 3-$CF_3$ | 19.20 | >500 | 321.05 |
| 17k | 2-F | 4-F | >500 | >500 | >500 |
| 17l | H | 2-F | 11.19 | 16.77 | 15.34 |
| 17m | H | 3-F | >500 | 37.24 | 106.84 |
| 17n | 2-$CH_3$ | 6-$CH_3$ | 415.21 | 134.67 | 334.72 |
| Sorafenib | | | 1.27 | 7.85 | 4.62 |

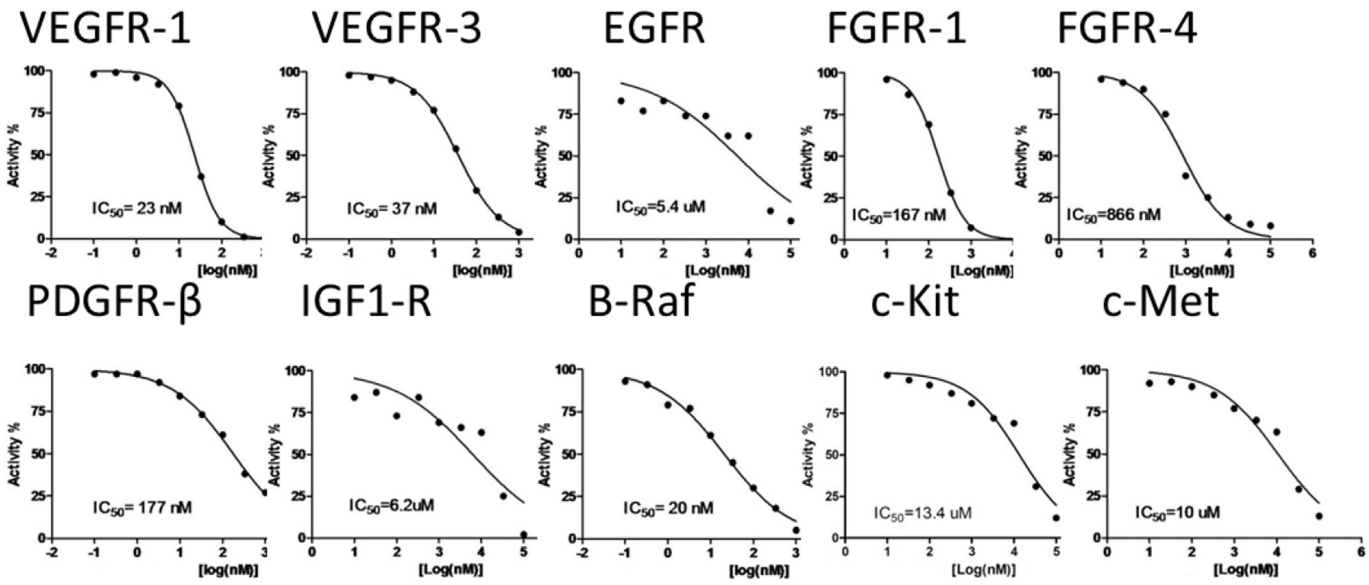


**Fig. 4.** The selectivity of **16a** against various RTKs.

human pancreatic cancerous cell lines (MIAPaCa-2), human epidermoid carcinoma cell line (A431), human gastric cancer cell line (MGC-803, MKN28), human thyroid cancer cell line (BCPAP), and human thyroid cancer cell lines (8505, K1). Highly consistent with the RTK inhibition, we are pleased to find that 16a significantly inhibited growth of all the nine cancer cell lines with $IC_{50}$ values ranging from 1.80 μM to 13.26 μM (Fig. 5). It displayed more superior anti-proliferative potency than sorafenib against eight cancer cell lines. The highest activity for 16a were found in human breast cancer cell lines human thyroid cancer cell lines (8505) with $IC_{50}$ values of 1.80 μM. In summary, 16a displayed significant anti-proliferative activity against a broad spectrum of cancer cell lines.

### 2.2.5. Molecular docking study

For further structural optimization and investigation of the potential binding mode, molecular modeling studies were performed using Sybyl-X (Version 2.0, Tripos Inc. St. Louis, MO). The most potent compound, 16a, was constructed and optimized using Powell's method with a Tripos force field. The molecular modeling was performed using Sybyl-X/Surflex-dock module, and the residues in a 5.0 Å radius around the natural ligand of VEGFR-2 (PDB ID: 4ASD), Tie-2 (PDB ID: 2P4I) and EphB4 (PDB ID: 2X9I) were selected as the active site. The binding mode of 16a with the ATP-pocket of VEGFR-2 (A), Tie-2 (B), EphB4 (C) were depicted in Figs. 6–8. As shown in Fig. 6, amine group of 1*H*-indazol-3-amine in 16a formed a hydrogen bond with Asp 1046 of VEGFR-2 with distance of 2.39 Å. In addition, the NH of thiourea formed one hydrogen bond with conserved Glu 885 for the bond length of 2.06 Å. As for Tie-2, the binding model was described in Fig. 7. 1*H*-indazol-3-amine also formed two hydrogen bonds with Ala 905 in hinge region of Tie-2 with the distance of 1.91 Å and 1.94 Å, respectively. The fluorine atoms at terminal aniline form two hydrogen bonds with Asp 982 with distances of 2.39 Å and 2.51 Å, respectively. Favorable binding interactions of 16a with the active site of EphB4 included four hydrogen bonds (Fig. 8): 1) the four hydrogen bonds forming between 1*H*-indazol-3-amine and Thr 693, Glu 694, and Met 696 in hinge region, the distance was 2.50 Å, 2.24 Å, 1.98 Å, and 1.84 Å, respectively; 2) another hydrogen bond forming between NH of urea and CO of Ile 621 with the distance of 1.87 Å. These molecular docking results indicated that the 1*H*-indazol-3-amine is beneficial for affinity of inhibitors with VEGFR-2, Tie-2, and EphB4. Interestingly, 1*H*-indazol-3-amine could be considered as novel hinge-binding group for further discovery of multi-target RTK inhibitors.

**Table 4**
Inhibition of compounds on human vascular endothelial cell viability ($IC_{50}$, μM).

| Compound | EA.hy 926 | Compound | EA. hy926 | Compound | EA. hy926 |
|---|---|---|---|---|---|
| 16a | 12.63 | 17e | 34.42 | 17n | 59.04 |
| 16b | 28.43 | 17f | 27.33 | 18a | 129.50 |
| 16c | 25.65 | 17g | 86.25 | 18b | 102.55 |
| 16d | 40.87 | 17h | 82.17 | 18c | 225.62 |
| 16e | 19.80 | 17i | 27.34 | 18d | 50.63 |
| 17a | 19.58 | 17j | 65.02 | 18e | 195.37 |
| 17b | 26.25 | 17k | 98.57 | 18f | 13.34 |
| 17c | 33.78 | 17l | 31.68 | 18g | 40.65 |
| 17d | 40.20 | 17m | 95.32 | Sorafenib | 18.52 |

## 3. Conclusion

In conclusion, a library of 26 novel multi-target inhibitors has been developed with promising activity on angiogenic and oncogenic VEGFR-2, Tie-2, and EphB4. Since these RTKs play essential roles in both angiogenesis and tumorigenesis. These candidates with a 'triplet' inhibition profile might have the major advantage of overcoming the compensatory feedback that characterize single-target drugs. *In vitro* RTK inhibition assay and molecular modelling revealed that these compounds could suppress VEGFR-2, Tie-2, and EphB4 kinase activity through preferential binding at the ATP-biding site. Biological evaluation using different models led to the discovery of a diaryl thiourea bearing 1*H*-indazol-3-amine (16a) which combined both anti-angiogenic and anticancer activities. Moreover, 1*H*-indazol-3-amine has been identified as an excellent hinge binding group for multi-target inhibitors of VEGFR-2, Tie-2, and EphB4. Further detailed action mechanism study and extensive pharmacokinetics evaluation of 16a are in progress and will be reported in due course.

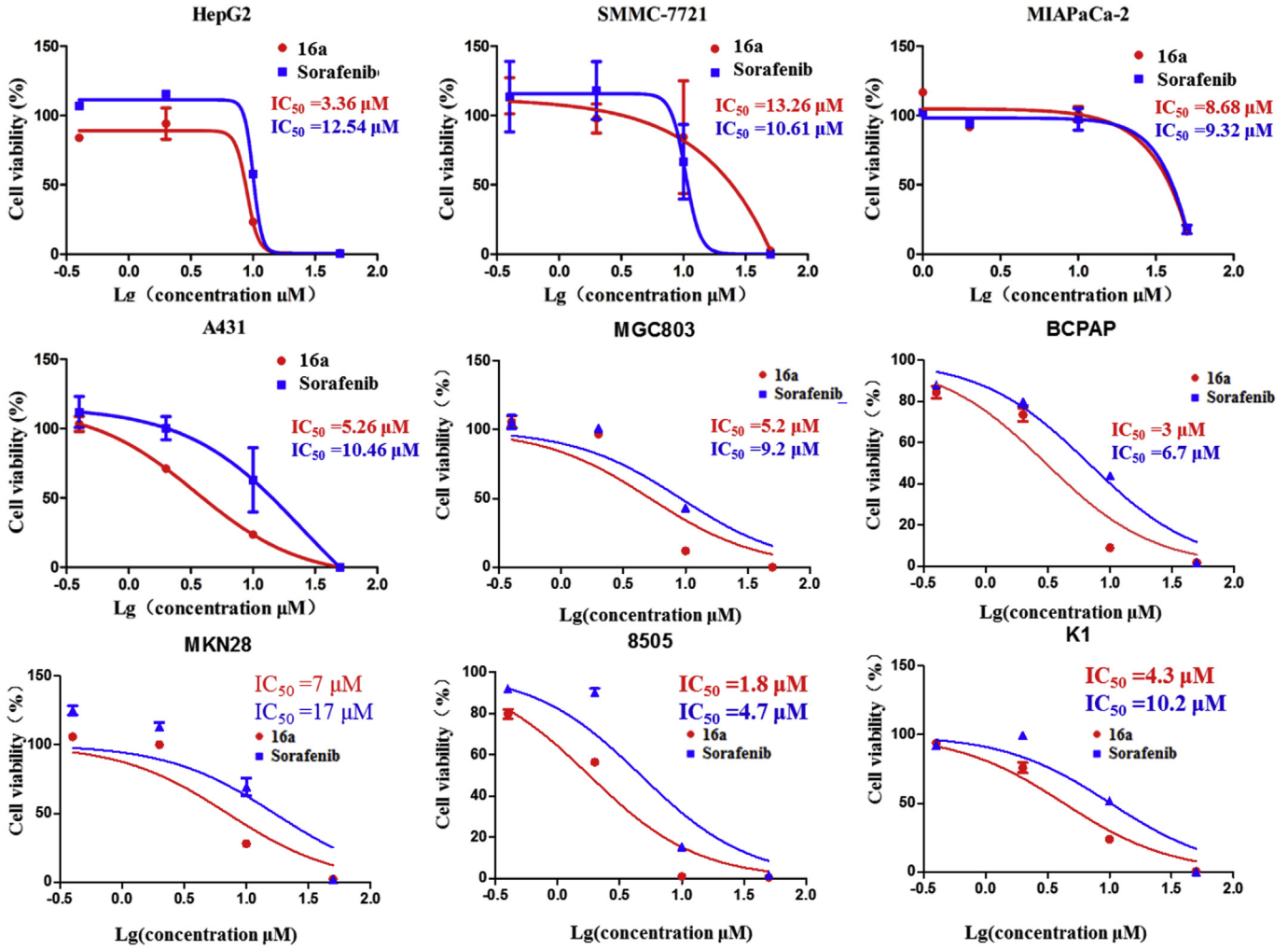


**Fig. 5.** Inhibition of **16a** (Red) on the growth of nine cancer cell lines compared with sorafenib (Blue). (For interpretation of the references to colour in this figure legend, the reader is referred to the web version of this article.)

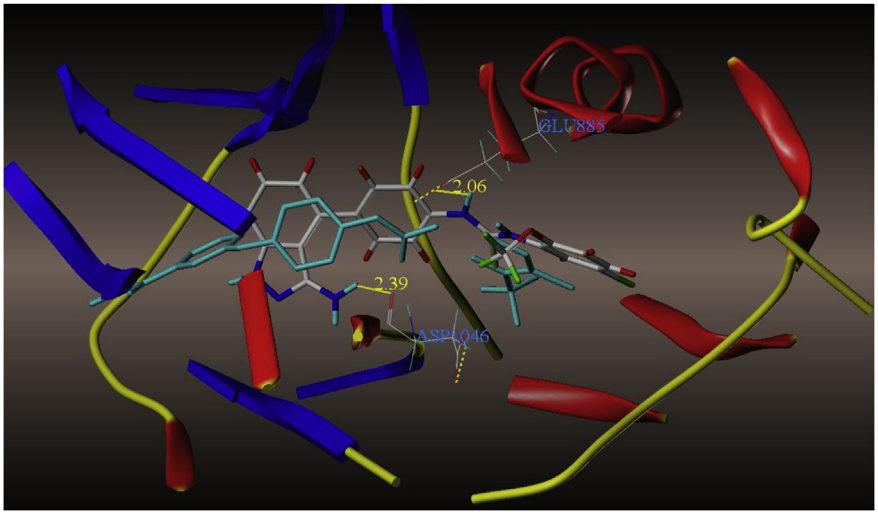


**Fig. 6.** Superimposition of the docking poses for VEGFR-2 (PDB ID: 4ASD) with compound (**16a**) and native ligand (cyan). Hydrogen bonds were depicted in dashed yellow lines. (For interpretation of the references to colour in this figure legend, the reader is referred to the web version of this article.)

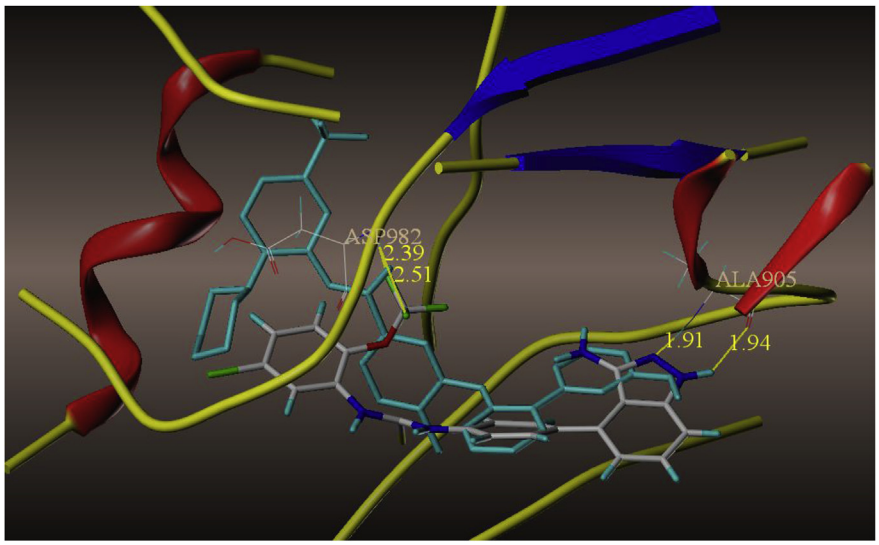


**Fig. 7.** Superimposition of the docking poses for Tie-2 (PDB ID: 2P4I) with compound (**16a**) and native ligand (cyan). Hydrogen bonds were depicted in dashed yellow lines. (For interpretation of the references to colour in this figure legend, the reader is referred to the web version of this article.)

## 4. Experimental section

### 4.1. Chemistry: general procedure

All reagents were purchased from commercial suppliers and purified according to the standard procedure. The reactions except those in aqueous media were carried out by standard techniques for the exclusion of moisture. All the reactions were monitored by thin layer chromatography (TLC) on 0.25-mm silica gel plates and visualized with UV light. Flash column chromatography was performed using silica gel (300–400 mesh). Melting points were determined using an electrothermal melting point apparatus and were uncorrected. $^{1}$H NMR and $^{13}$C NMR spectra were recorded on a Bruker Advance AC 400 instrument at 400 MHz and 101 MHz, respectively. Chemical shift ($\delta$) were reported in parts per million (ppm) with TMS as an internal standard and coupling constants (J) were expressed in hertz (Hz). High resolution mass spectra (HRMS) analysis was performed on a Shimadzu LCMS-IF-TOF instrument. All the title compounds were determined to be $\geq$ 95% pure by HPLC analysis which was carried out on a Shimadzu HPLC instrument.

#### 4.1.1. General procedure for the synthesis of diaryl thiourea derivatives 16a-16e

*4.1.1.1. 4-Iodine -1H-indazol-3-ylamine (2).* 2-Fluoro-6-iodobenzonitrile **1** (10.0 g, 40 mmol) and $Na_2CO_3$(5.2 g, 62 mmol) were suspended in ethanol (70 mL), hydrazine hydrate (12.5 mL) was added. The resulting mixture was heated to reflux and stirred for 8 h. After cooling to r.m., 50 mL water was added and the reaction mixture was allowed to stir for another 2 h at r.m. and 2 h at 0 °C. The product was collected by filtration, washed with water and dried under vacuum to give 4-iodine-1*H*-indazol-3-ylamine **2** as yellow solid (8.0 g, 77%).

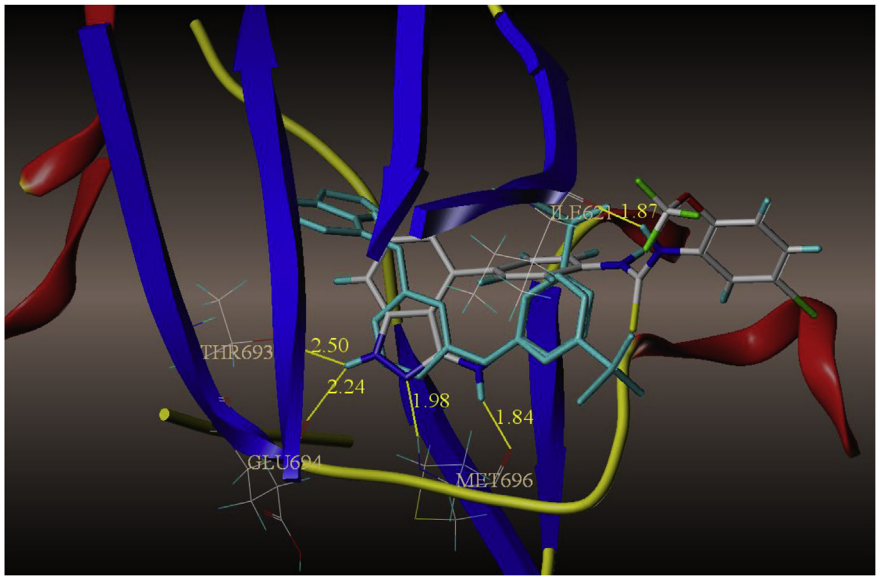


**Fig. 8.** Superimposition of the docking poses for EphB4 (PDB ID: 2X9F) with compound (**16a**) and native ligand (cyan). Hydrogen bonds were depicted in dashed yellow lines. (For interpretation of the references to colour in this figure legend, the reader is referred to the web version of this article.)

*4.1.1.2. 4-(4-aminophenyl)-1H-indazol-3-amine (4).* $Pd(PPh_3)_4$ (3.3 g, 2.89 mmol) was added to a degassed solution of 4-aminophenyl boronic acid **3** (5.0 g, 28.9 mmol), potassium carbonate (9.2 g, 86.7 mmol), 4-iodine-1*H*-indazol-3-ylamine **2** (7.5 g, 28.9 mmol) in 150 mL 1,4-dioxane and 50 mL water. The reaction mixture was heated at 90 °C in an oil bath and stirred under nitrogen for 24 h. The mixture was dissolved in $H_2O$ and then extracted with ethyl acetate (30 mL × 3). The combined organic layer was washed with brine, dried over $Na_2SO_4$ for overnight, filtered, and concentrated *in vacuo* to give the crude product, which was isolated by silica gel flash chromatography (Petroleum ether (PE)/Ethyl acetate (AcOEt) = 3:1) to obtain **4** as white solid (3.2g, yield 45%).

*4.1.1.3. (3-Bromo-5-(trifluoromethyl)phenyl)carbamodithioic acid (5).* 3-Bromo-5-(trifluoromethyl)aniline (2.5 g, 10.4 mmol), 1,4-diazabicyclo [2.2.2]octane (DABCO, 1.4 g, 12.5 mmol) was dissolved in toluene (40 mL). Then 1.9 mL carbon disulphide was added dropwise to the above mixture. Subsequently, the mixture was reacted at room temperature for 8 h. The product was collected by filtration and dried under vacuum to afford **5** as slight yellow solid (1.2 g, 40%).

*4.1.1.4. 1-Bromo-3-isothiocyanato-5-(trifluoromethyl) benzene (6).* Compound **5** (0.8 g, 2.5 mmol) was dissolved in anhydrous $CH_2Cl_2$ (20 mL). Then triphosgene (BTC, 0.88 g, 3 mmol) in anhydrous $CH_2Cl_2$ was added dropwise to the above mixture on the ice-bath, and stirring continued for 2 h at room temperature. After completion of the reaction, the organic layer was washed with water and brine (100 mL × 3), and dried over $Na_2SO_4$. After filtration and concentration *in vacuo*, the residue was purified by silica gel flash chromatography to afford **6** (0.50 g, 30.0%).

*4.1.1.5. N-[4-(3-amino-1H-indazol-4-yl)phenyl]-N'-[5-bromo-2-(trifluoromethoxy)phenyl]thiourea (16a).* The key intermediate **4** (0.80 g, 2.84 mmol) was dissolved in anhydrous $CH_2Cl_2$ (10 mL). 1-Bromo-3-isothiocyanato-5-(trifluoromethyl)benzene **6** in anhydrous $CH_2Cl_2$ (10 mL) was added dropwise to the above mixture, and stirring on the ice-bath continued for 2 h. After stirring at room temperature for 18 h. The organic layer was washed with water and brine (100 mL × 3), and dried over $Na_2SO_4$. After filtration and concentration *in vacuo*, the residue was purified by silica gel flash chromatography to yield **16a** in 30% yield. As a white solid, HRMS *m/z* calcd for $C_{21}H_{15}BrF_3N_5OS$ ($[M+H]^+$) 522.0211, found 522.0154. m.p. = 111–112 °C, $^1$H NMR (400 MHz, DMSO) $\delta$ 11.79 (s, 1H), 10.34 (s, 1H), 9.65 (s, 1H), 8.03 (d, $J$ = 2.4 Hz, 1H), 7.64 (d, $J$ = 8.4 Hz, 2H), 7.56 (m, 1H), 7.48 (d, $J$ = 8.5 Hz, 2H), 7.42 (m, 1H), 7.30 (d, $J$ = 2.0 Hz, 1H), 7.29 (s, 1H), 6.82 (m, 1H), 4.40 (s, 2H).$^{13}$C NMR (101 MHz, DMSO) $\delta$ 180.66, 148.53, 142.50, 138.80, 136.25, 135.55, 134.06, 132.01, 130.19, 129.60, 126.72, 124.01, 123.45, 121.69, 119.63, 119.34, 110.79, 109.36.

The title compounds **16b-16e** were prepared from the key intermediate **4** and **6** with a similar procedure as described for compound **16a**.

*4.1.1.6. N-[4-(3-amino-1H-indazol-4-yl)phenyl]-N'-[2-bromo-5-(trifluoromethoxy)phenyl]thiourea (16b).* HRMS *m/z* calcd for $C_{21}H_{15}BrF_3N_5OS$ ($[M]^+$) 521.0133, found 524.0138. m.p. = 161–162 °C, $^1$H NMR (400 MHz, DMSO) $\delta$ 10.44 (s, 1H), 9.62 (s, 1H), 7.83 (d, $J$ = 8.8 Hz, 1H), 7.69 (s, 2H), 7.67 (s, 1H), 7.49 (d, $J$ = 8.4 Hz, 2H), 7.31 (d, $J$ = 2.2 Hz, 1H), 7.29 (d, $J$ = 5.5 Hz, 1H), 7.25 (m, 1H), 6.86–6.82 (m, 1H).$^{13}$C NMR (101 MHz, DMSO) $\delta$ 180.43, 148.17, 147.51, 142.53, 140.08, 138.68, 136.22, 135.57, 134.31, 129.67, 126.86, 124.18, 123.07, 120.83, 120.29, 119.76, 110.79, 109.42.

*4.1.1.7. N-[4-(3-amino-1H-indazol-4-yl)phenyl]-N'-(2,4-dichlorophenyl)thiourea (16c).* HRMS *m/z* calcd for $C_{20}H_{15}Cl_2N_5S$ ($[M+H]^+$) 428.0425, found 428.0471. m.p. = 116–117 °C, $^1$H NMR (400 MHz, DMSO) $\delta$ 11.78 (s, 1H), 10.23 (s, 1H), 9.57 (s, 1H), 7.72 (d, $J$ = 2.4 Hz, 1H), 7.63 (d, $J$ = 8.4 Hz, 2H), 7.60 (d, $J$ = 8.6 Hz, 1H), 7.49–7.46 (m, 2H), 7.44 (d, $J$ = 2.4 Hz, 1H), 7.29 (d, $J$ = 2.5 Hz, 1H), 7.28 (s, 1H), 6.82 (m, 1H), 4.42 (s, 2H).$^{13}$C NMR (101 MHz, DMSO) $\delta$ 180.77, 148.54, 142.50, 138.82, 136.34, 136.16, 135.59, 132.16, 131.72, 131.56, 129.63, 129.42, 127.90, 126.72, 124.16, 119.60, 110.78, 99.99.

*4.1.1.8. N-[4-(3-amino-1H-indazol-4-yl)phenyl]-N'-(3,4-difluorophenyl)thiourea (16d).* HRMS *m/z* calcd for $C_{20}H_{15}F_2N_5S$ ($[M+H]^+$) 396.1016, found 396.1035. m.p. = 112–113 °C, $^1$H NMR (400 MHz, DMSO) $\delta$ 11.78 (s, 1H), 10.12 (s, 1H), 9.96 (s, 1H), 7.71 (m, 1H), 7.59 (d, $J$ = 8.4 Hz, 2H), 7.46 (d, $J$ = 8.4 Hz, 2H), 7.44–7.38 (m, 1H), 7.32–7.21 (m, 3H), 6.82 (m, 1H), 4.41 (s, 2H).$^{13}$C NMR (101 MHz, DMSO) $\delta$ 180.20, 148.54, 142.49, 138.98, 136.94, 135.98, 135.61, 129.58, 126.72, 124.02, 121.18, 119.60, 117.52, 117.34, 114.00, 113.81, 110.80, 109.32.

*4.1.1.9. N-[4-(3-amino-1H-indazol-4-yl)phenyl]-N'-(3,4-dichlorophenyl)thiourea (16e).* HRMS *m/z* calcd for $C_{20}H_{15}Cl_2N_5S$ ($[M+H]^+$) 428.0425, found 428.0472. m.p. = 121–122 °C, $^1$H NMR (400 MHz, DMSO) $\delta$ 11.78 (s, 1H), 10.22 (s, 1H), 10.05 (s, 1H), 7.90 (d, $J$ = 2.4 Hz, 1H), 7.62 (s, 1H), 7.59 (d, $J$ = 6.8 Hz, 2H), 7.49 (d, $J$ = 2.4 Hz, 1H), 7.47 (d, $J$ = 2.3 Hz, 1H), 7.46 (d, $J$ = 3.2 Hz, 1H), 7.32–7.27 (m, 2H), 6.85–6.79 (m, 1H), 4.41 (s, 2H).$^{13}$C NMR (101 MHz, DMSO) $\delta$ 179.99, 148.53, 142.49, 140.28, 138.89, 136.07, 135.58, 130.89, 130.65, 129.62, 126.73, 126.55, 125.55, 124.32, 124.00, 119.62, 110.79, 109.33.

*4.1.2. General procedure for the synthesis of N-(pyridin-2-yl) acrylamide diaryl urea derivatives 17a-17n*

*4.1.2.1. 1-(4-(tert-butyl)phenyl)-3-(4-(4,4,5,5-tetramethyl-1,3,2-dioxaborolan-2-yl)phenyl)urea (8).* Triphosgene (1.77 g, 6.03 mmol) was dissolved in anhydrous $CH_2Cl_2$ (30 mL) and the mixture was stirred on the ice-bath for 5 min. *Tert*-butyl-aniline (2.0 g, 13.4 mmol) in anhydrous $CH_2Cl_2$ was added dropwise to the mixture and stirring was continued for 15 min. Then triethanolamine (2.2 mL, 16.1 mmol) diluted with $CH_2Cl_2$ (20 mL) was added onto the mixture. Stirring was continued for 15 min, a solution of triethanolamine (2.2 mL, 16.1 mmol) and 4-(4,4,5,5-tetramethyl-1,3,2-dioxaborolan-2-yl)aniline **7** (2.35 g, 10.72 mmol) in anhydrous $CH_2Cl_2$ (30 mL) was added and continued stirring for 20min. Subsequently, the ice bath was removed, and the mixture was reacted at room temperature overnight. After completion of the action, the reaction was quenched with dilute $NaHCO_3$.The organic layer was washed with water and brine, and dried over $Na_2SO_4$. After filtration and concentration *in vacuo*, the residue was purified by silica gel flash chromatography (PE/AcOEt = 3:1) yielding **8** as white solid (3.4 g, 64.4%).

*4.1.2.2. 1-(4-(6-aminopyridin-2-yl)phenyl)-3-(3-(tert-butyl)phenyl) urea (10).* A flask charged with $Pd(PPh_3)_4$ (0.30 g, 0.26 mmol), potassium carbonate (1.71 g, 5.26 mmol), and intermediate **8** (1.00 g, 2.63 mmol) and 2-amino-6-bromopyridine **9** (0.45 g, 2.63 mmol) were flushed with nitrogen and suspended in 1,4-dioxane (90 mL) and water (30 mL). The mixture was then refluxed overnight under nitrogen. The hot suspension was filtered and the filtrate distilled by rotary evaporation to remove 1,4-dioxane. Water (50 mL) was added and the product was extracted with AcOEt (30 mL × 3), washed with water, and dried over $Na_2SO_4$. After filtration and concentration *in vacuo*, the residue was purified by silica gel flash chromatography (PE/AcOEt = 3:1) affording **10**

(0.56 g, 45.5%) as yellow solid.

*4.1.2.3. N-(6-(4-(3-(4-chloro-3-(trifluoromethyl)phenyl) ureido) phenyl)pyridin-2-yl)acrylamide (17a).* To a mixture of **10** (0.20 g, 0.55 mmol) and triethanolamine (0.31 mL, 2.20 mmol) dissolved in 20 mL of anhydrous THF in ice-bath. After stirring for 30 min, acryloyl chloride (0.11 mL, 1.33 mmol) was dropped. The reaction was warmed to the room temperature and stirred overnight. After the completion of the reaction, the mixture was filtered and the filtrate distilled by rotary evaporation to remove THF. After filtration and concentration *in vacuo*, the residues was purified by silica gel flash chromatography (PE/AcOEt = 1:1) yielding **17a** as white solid (yield 55.3%), HRMS *m/z* calcd for $C_{22}H_{16}ClF_3N_4O_2$ ($[M]^+$) 460.0914, found 460.9698. m.p. = 165–167 °C, $^1$H NMR (400 MHz, DMSO) $\delta$ 10.69 (s, 1H), 9.24 (s, 1H), 9.06 (s, 1H), 8.15 (d, $J$ = 2.2 Hz, 1H), 8.12 (d, $J$ = 8.2 Hz, 1H), 8.05 (d, $J$ = 8.8 Hz, 2H), 7.86 (t, $J$ = 8.0 Hz, 1H), 7.65 (d, $J$ = 1.8 Hz, 2H), 7.63 (d, $J$ = 4.4 Hz, 1H), 7.60 (s, 1H), 6.70 (m, $J$ = 17.0, 10.2 Hz, 1H), 6.34 (m, $J$ = 17.0, 1.9 Hz, 1H), 5.81 (m, $J$ = 10.2, 1.9 Hz, 1H). $^{13}$C NMR (101 MHz, DMSO) $\delta$ 164.26, 155.01, 152.76, 152.11, 140.76, 139.72, 139.62, 132.49, 132.12, 128.18, 127.66, 127.35, 127.04, 123.62, 122.91, 118.82, 117.32, 115.70, 112.37.

The title compounds **17b-17n** were prepared from the key intermediate **10** and acryloyl chloride with a similar procedure as described for compounds **17b**.

*4.1.2.4. N-(6-(4-(3-(4-chloro-3-methylphenyl)ureido)phenyl) pyridin-2-yl)acrylamide (17b).* White solid (yield 78.1%), HRMS *m/z* calcd for $C_{22}H_{19}ClN_4O_2$ ($[M]^+$) 406.1197, found 406.9239. m.p. = 217–219 °C, $^1$H NMR (400 MHz, DMSO) $\delta$ 10.68 (s, 1H), 8.91 (s, 1H), 8.83 (s, 1H), 8.11 (d, $J$ = 8.2 Hz, 1H), 8.04 (d, $J$ = 8.7 Hz, 2H), 7.85 (t, $J$ = 7.9 Hz, 1H), 7.73 (d, $J$ = 1.9 Hz, 1H), 7.65–7.62 (m, 1H), 7.59 (d, $J$ = 8.7 Hz, 2H), 7.26 (d, $J$ = 8.3 Hz, 1H), 7.21 (m, $J$ = 8.3, 2.0 Hz, 1H), 6.70 (m, $J$ = 17.0, 10.2 Hz, 1H), 6.34 (m, $J$ = 17.0, 1.8 Hz, 1H), 5.84–5.77 (m, 1H), 2.27 (s, 3H). $^{13}$C NMR (101 MHz, DMSO) $\delta$ 164.26, 155.07, 152.78, 152.09, 141.09, 139.59, 139.23, 133.61, 132.13, 131.65, 129.28, 128.85, 128.16, 127.65, 118.68, 118.53, 117.51, 115.63, 112.29, 19.29.

*4.1.2.5. N-(6-(4-(3-(4-fluorophenyl)ureido)phenyl)pyridin-2-yl) acrylamide (17c).* White solid (yield 81.8%), HRMS *m/z* calcd for $C_{21}H_{17}FN_4O_2$ ($[M]^+$) 376.1336, found 376.9211. m.p. = 252–254 °C, $^1$H NMR (400 MHz, DMSO) $\delta$ 10.68 (s, 1H), 8.87 (s, 1H), 8.78 (s, 1H), 8.11 (d, $J$ = 8.2 Hz, 1H), 8.03 (d, $J$ = 8.7 Hz, 2H), 7.85 (t, $J$ = 8.0 Hz, 1H), 7.63 (d, $J$ = 7.7 Hz, 1H), 7.59 (d, $J$ = 8.7 Hz, 2H), 7.52–7.46 (m, 2H), 7.14 (t, $J$ = 8.9 Hz, 2H), 6.70 (m, $J$ = 17.0, 10.2 Hz, 1H), 6.34 (m, $J$ = 17.0, 1.8 Hz, 1H), 5.81 (m, $J$ = 10.2, 1.8 Hz, 1H). $^{13}$C NMR (101 MHz, DMSO) $\delta$ 164.25, 159.08, 156.71, 155.10, 152.97, 152.09, 141.25, 139.59, 136.37, 132.13, 132.05, 128.17, 127.65, 120.59, 120.52, 118.45, 115.88, 115.66, 112.26.

*4.1.2.6. N-(6-(4-(3-(4-(tert-butyl)phenyl)ureido)phenyl) pyridin-2-yl)acrylamide (17d).* White solid (yield 84.0%), HRMS *m/z* calcd for $C_{25}H_{26}N_4O_2$ ($[M+H]^+$) 415.2056, found 415.0150. m.p. = 194–196 °C, $^1$H NMR (400 MHz, DMSO) $\delta$ 10.68 (s, 1H), 8.83 (s, 1H), 8.65 (s, 1H), 8.11 (d, $J$ = 8.2 Hz, 1H), 8.03 (d, $J$ = 8.7 Hz, 2H), 7.85 (t, $J$ = 8.0 Hz, 1H), 7.66–7.61 (m, 1H), 7.61 (s, 2H), 7.39 (d, $J$ = 8.7 Hz, 2H), 7.31 (d, $J$ = 8.7 Hz, 2H), 6.70 (m, $J$ = 17.0, 10.2 Hz, 1H), 6.37–6.31 (m, 1H), 5.81 (m, $J$ = 10.2, 1.8 Hz, 1H), 1.27 (s, 9H). $^{13}$C NMR (101 MHz, DMSO) $\delta$ 164.26, 155.13, 152.90, 152.08, 144.77, 141.38, 139.58, 137.38, 132.13, 131.92, 128.17, 127.66, 125.88, 118.61, 118.32, 115.60, 112.24, 34.36, 31.72.

*4.1.2.7. N-(6-(4-(3-(2-chlorophenyl)ureido)phenyl)pyridin-2-yl) acrylamide (17e).* White solid (yield 46.9%), HRMS *m/z* calcd for $C_{21}H_{17}ClN_4O_2$ ($[M]^+$) 392.1040, found 392.8999. m.p. = 178–180 °C, $^1$H NMR (400 MHz, DMSO) $\delta$ 10.69 (s, 1H), 9.62 (s, 1H), 8.38 (s, 1H), 8.21–8.16 (m, 1H), 8.11 (d, $J$ = 8.2 Hz, 1H), 8.06 (d, $J$ = 8.7 Hz, 2H), 7.86 (t, $J$ = 8.0 Hz, 1H), 7.64 (d, $J$ = 7.7 Hz, 1H), 7.60 (d, $J$ = 8.7 Hz, 2H), 7.48 (m, $J$ = 8.0, 1.1 Hz, 1H), 7.32 (m, $J$ = 11.5, 4.2 Hz, 1H), 7.09–7.02 (m, 1H), 6.70 (m, $J$ = 17.0, 10.2 Hz, 1H), 6.34 (m, $J$ = 17.0, 1.8 Hz, 1H), 5.81 (m, $J$ = 10.2, 1.7 Hz, 1H). $^{13}$C NMR (101 MHz, DMSO) $\delta$ 164.26, 155.03, 152.49, 152.10, 140.97, 139.64, 136.30, 132.33, 132.12, 129.72, 128.20, 128.08, 127.76, 123.94, 122.53, 121.88, 118.43, 115.65, 112.32.

*4.1.2.8. N-(6-(4-(3-(3-isopropylphenyl)ureido)phenyl) pyridin-2-yl) acrylamide (17f).* White solid (yield 76.5%), HRMS *m/z* calcd for $C_{24}H_{24}N_4O_2$ ($[M]^+$) 400.1899, found 400.9910. m.p. = 172–174 °C, $^1$H NMR (400 MHz, DMSO) $\delta$ 10.69 (s, 1H), 8.89 (s, 1H), 8.73 (s, 1H), 8.12 (d, $J$ = 8.2 Hz, 1H), 8.03 (d, $J$ = 8.7 Hz, 2H), 7.85 (t, $J$ = 8.0 Hz, 1H), 7.63 (d, $J$ = 7.7 Hz, 1H), 7.60 (d, $J$ = 8.7 Hz, 2H), 7.39 (s, 1H), 7.28 (d, $J$ = 8.2 Hz, 1H), 7.20 (t, $J$ = 7.8 Hz, 1H), 6.88 (d, $J$ = 7.5 Hz, 1H), 6.71 (m, $J$ = 17.0, 10.2 Hz, 1H), 6.34 (m, $J$ = 17.0, 1.8 Hz, 1H), 5.81 (m, $J$ = 10.2, 1.8 Hz, 1H), 2.85 (t, $J$ = 13.8, 6.9 Hz, 1H), 1.21 (d, $J$ = 6.9 Hz, 6H). $^{13}$C NMR (101 MHz, DMSO) $\delta$ 164.26, 155.13, 152.88, 152.09, 149.53, 141.34, 140.01, 139.58, 132.14, 131.96, 129.16, 128.15, 127.65, 120.51, 118.36, 116.71, 116.37, 115.61, 112.25, 33.98, 24.35.

*4.1.2.9. N-(6-(4-(3-(3-chlorophenyl)ureido)phenyl)pyridin-2-yl) acrylamide (17g).* White solid (yield 69.7%), HRMS *m/z* calcd for $C_{21}H_{17}ClN_4O_2$ ($[M]^+$) 392.1040, found 392.9003. m.p. = 214–216 °C, $^1$H NMR (400 MHz, DMSO) $\delta$ 10.68 (s, 1H), 8.98 (s, 2H), 8.12 (d, $J$ = 8.2 Hz, 1H), 8.04 (d, $J$ = 8.7 Hz, 2H), 7.86 (t, $J$ = 8.0 Hz, 1H), 7.76 (s, 1H), 7.64 (d, $J$ = 7.6 Hz, 1H), 7.60 (d, $J$ = 8.8 Hz, 2H), 7.33 (d, $J$ = 8.1 Hz, 1H), 7.30 (d, $J$ = 1.5 Hz, 1H), 7.04 (m, $J$ = 7.3, 1.8 Hz, 1H), 6.70 (m, $J$ = 17.0, 10.2 Hz, 1H), 6.34 (m, $J$ = 17.0, 1.8 Hz, 1H), 5.81 (m, $J$ = 10.2, 1.8 Hz, 1H). $^{13}$C NMR (101 MHz, DMSO) $\delta$ 164.26, 155.05, 152.74, 152.10, 141.62, 140.98, 139.61, 133.69, 132.29, 132.13, 130.88, 128.17, 127.67, 122.05, 118.60, 118.12, 117.20, 115.65, 112.31.

*4.1.2.10. N-(6-(4-(3-(4-(trifluoromethoxy)phenyl)ureido) phenyl) pyridin-2-yl)acrylamide (17h).* White solid (yield 81.3%), HRMS *m/z* calcd for $C_{22}H_{17}F_3N_4O_3$ ($[M]^+$) 442.1253, found 442.9702. m.p. = 248–250 °C, $^1$H NMR (400 MHz, DMSO) $\delta$ 10.68 (s, 1H), 9.00 (s, 1H), 8.97 (s, 1H), 8.12 (d, $J$ = 8.2 Hz, 1H), 8.04 (d, $J$ = 8.7 Hz, 2H), 7.85 (t, $J$ = 8.0 Hz, 1H), 7.63 (d, $J$ = 7.9 Hz, 1H), 7.61 (d, $J$ = 3.1 Hz, 2H), 7.59 (d, $J$ = 3.4 Hz, 2H), 7.31 (d, $J$ = 8.5 Hz, 2H), 6.71 (m, $J$ = 17.0, 10.2 Hz, 1H), 6.34 (m, $J$ = 17.0, 1.9 Hz, 1H), 5.81 (m, $J$ = 10.2, 1.8 Hz, 1H). $^{13}$C NMR (101 MHz, DMSO) $\delta$ 164.26, 155.08, 152.84, 152.10, 143.16, 141.09, 139.59, 139.37, 132.21, 132.13, 128.15, 127.66, 122.20, 119.95, 118.54, 115.64, 112.30.

*4.1.2.11. N-(6-(4-(3-(2,4-dichlorophenyl)ureido)phenyl) pyridin-2-yl) acrylamide (17i).* White solid (yield 62.4%), HRMS *m/z* calcd for $C_{21}H_{16}Cl_2N_4O_2$ ($[M]^+$) 426.0650, found 426.8830. m.p. = 243–245 °C, $^1$H NMR (400 MHz, DMSO) $\delta$ 10.69 (s, 1H), 9.65 (s, 1H), 8.46 (s, 1H), 8.23 (d, $J$ = 8.9 Hz, 1H), 8.12 (d, $J$ = 8.1 Hz, 1H), 8.06 (d, $J$ = 8.5 Hz, 2H), 7.86 (t, $J$ = 7.9 Hz, 1H), 7.64 (d, $J$ = 3.5 Hz, 1H), 7.63 (s, 1H), 7.60 (d, $J$ = 8.5 Hz, 2H), 7.41 (m, $J$ = 8.9, 1.8 Hz, 1H), 6.70 (m, $J$ = 17.0, 10.2 Hz, 1H), 6.34 (d, $J$ = 16.9 Hz, 1H), 5.81 (d, $J$ = 10.7 Hz, 1H). $^{13}$C NMR (101 MHz, DMSO) $\delta$ 164.26, 154.99, 152.36, 152.10, 140.78, 139.63, 135.57, 132.48, 132.11, 129.05, 128.19, 128.13, 127.77, 126.73, 123.22, 122.67, 118.51, 115.67, 112.36.

*4.1.2.12. N-(6-(4-(3-(3-(trifluoromethyl)phenyl)ureido) phenyl) pyridin-2-yl)acrylamide (17j).* White solid (yield 71.9%), HRMS *m/z* calcd for $C_{22}H_{17}F_3N_4O_2$ ($[M]^+$) 426.1304, found 426.9488. m.p. = 179–180 °C, $^1$H NMR (400 MHz, DMSO) $\delta$ 10.70 (s, 1H), 9.13 (s, 1H), 9.02 (s, 1H), 8.13 (d, $J$ = 8.2 Hz, 1H), 8.07 (s, 1H), 8.05 (d, $J$ = 8.9 Hz, 2H), 7.86 (t, $J$ = 8.0 Hz, 1H), 7.64 (d, $J$ = 6.6 Hz, 2H), 7.60 (d, $J$ = 8.5 Hz, 2H), 7.53 (t, $J$ = 8.0 Hz, 1H), 7.33 (d, $J$ = 7.6 Hz, 1H), 6.71

(m, $J$ = 17.0, 10.2 Hz, 1H), 6.35 (m, $J$ = 17.0, 1.8 Hz, 1H), 5.81 (m, $J$ = 10.2, 1.8 Hz, 1H). $^{13}$C NMR (101 MHz, DMSO) $\delta$ 164.27, 155.05, 152.86, 152.11, 140.93, 139.59, 132.36, 132.14, 130.38, 130.19, 129.88, 128.14, 127.66, 126.04, 123.33, 122.38, 118.69, 115.66, 114.69, 112.34.

*4.1.2.13. N-(6-(4-(3-(2,4-difluorophenyl)ureido)phenyl) pyridin-2-yl) acrylamide (17k).* White solid (yield 81.3%), HRMS $m/z$ calcd for $C_{21}H_{16}F_2N_4O_2$ ($[M]^+$) 394.1241, found 394.9205. m.p. = 189–191 °C, $^1$H NMR (400 MHz, DMSO) $\delta$ 10.68 (s, 1H), 8.97 (s, 1H), 8.96 (s, 1H), 8.12 (d, $J$ = 8.0 Hz, 1H), 8.04 (d, $J$ = 8.5 Hz, 2H), 7.85 (t, $J$ = 7.9 Hz, 1H), 7.70 (m, $J$ = 11.0, 7.5 Hz, 1H), 7.63 (d, $J$ = 7.7 Hz, 1H), 7.59 (d, $J$ = 8.6 Hz, 2H), 7.36 (m, $J$ = 19.4, 9.3 Hz, 1H), 7.15 (d, $J$ = 8.3 Hz, 1H), 6.71 (m, $J$ = 16.9, 10.2 Hz, 1H), 6.35 (d, $J$ = 16.9 Hz, 1H), 5.81 (d, $J$ = 11.2 Hz, 1H). $^{13}$C NMR (101 MHz, DMSO) $\delta$ 164.26, 155.06, 152.81, 152.10, 140.97, 139.59, 137.25, 132.29, 132.13, 128.16, 127.66, 118.62, 117.95, 117.77, 115.65, 114.96, 112.32, 107.85, 107.63.

*4.1.2.14. N-(6-(4-(3-(2-fluorophenyl)ureido)phenyl)pyridin-2-yl) acrylamide (17l).* White solid (yield 65.7%), HRMS $m/z$ calcd for $C_{21}H_{17}FN_4O_2$ ($[M]^+$) 376.1336, found 376.9198. m.p. = 214–216 °C, $^1$H NMR (400 MHz, DMSO) $\delta$ 10.69 (s, 1H), 9.27 (s, 1H), 8.63 (d, $J$ = 2.3 Hz, 1H), 8.18 (td, $J$ = 8.2, 1.4 Hz, 1H), 8.12 (d, $J$ = 8.2 Hz, 1H), 8.05 (d, $J$ = 8.7 Hz, 2H), 7.86 (t, $J$ = 8.0 Hz, 1H), 7.64 (d, $J$ = 7.7 Hz, 1H), 7.59 (d, $J$ = 8.7 Hz, 2H), 7.30–7.22 (m, 1H), 7.16 (t, $J$ = 7.7 Hz, 1H), 7.08–6.98 (m, 1H), 6.70 (m, $J$ = 17.0, 10.2 Hz, 1H), 6.34 (m, $J$ = 17.0, 1.8 Hz, 1H), 5.81 (m, $J$ = 10.2, 1.8 Hz, 1H). $^{13}$C NMR (101 MHz, DMSO) $\delta$ 164.26, 155.05, 153.73, 152.54, 152.10, 151.34, 140.97, 139.62, 132.28, 132.13, 128.18, 127.75, 125.00, 123.06, 121.09, 118.35, 115.66, 115.38, 112.32.

*4.1.2.15. N-(6-(4-(3-(3-fluorophenyl)ureido)phenyl)pyridin-2-yl) acrylamide (17m).* White solid (yield 69.7%), HRMS $m/z$ calcd for $C_{21}H_{17}FN_4O_2$ ($[M]^+$) 376.1336, found 376.9199. m.p. = 211–213 °C, $^1$H NMR (400 MHz, DMSO) $\delta$ 10.68 (s, 1H), 8.99 (s, 1H), 8.96 (s, 1H), 8.11 (d, $J$ = 8.2 Hz, 1H), 8.04 (d, $J$ = 8.7 Hz, 2H), 7.86 (t, $J$ = 8.0 Hz, 1H), 7.64 (d, $J$ = 7.7 Hz, 1H), 7.60 (d, $J$ = 8.8 Hz, 2H), 7.53 (m, $J$ = 12.0, 2.2 Hz, 1H), 7.32 (m, $J$ = 15.2, 8.1 Hz, 1H), 7.15 (m, $J$ = 8.2, 1.1 Hz, 1H), 6.81 (td, $J$ = 8.4, 2.2 Hz, 1H), 6.70 (m, $J$ = 17.0, 10.2 Hz, 1H), 6.34 (m, $J$ = 17.0, 1.8 Hz, 1H), 5.81 (m, $J$ = 10.2, 1.8 Hz, 1H). $^{13}$C NMR (101 MHz, DMSO) $\delta$ 164.26, 164.08, 161.69, 155.06, 152.73, 152.10, 141.99, 141.88, 140.99, 139.61, 132.28, 132.13, 130.86, 130.76, 128.17, 127.67, 118.58, 115.66, 114.49, 112.31, 108.85, 108.64, 105.55, 105.28.

*4.1.2.16. N-(6-(4-(3-(2,6-dimethylphenyl)ureido)phenyl) pyridin-2-yl)acrylamide (17n).* White solid (yield 10.0%), HRMS $m/z$ calcd for $C_{23}H_{22}N_4O_2$ ($[M]^+$) 386.1743, found 386.9664. m.p. = 200–202 °C, $^1$H NMR (400 MHz, DMSO) $\delta$ 10.67 (s, 1H), 8.97 (s, 1H), 8.10 (d, $J$ = 8.1 Hz, 1H), 8.02 (d, $J$ = 8.5 Hz, 2H), 7.86 (d, $J$ = 7.7 Hz, 1H), 7.81 (d, $J$ = 10.6 Hz, 1H), 7.63 (s, 1H), 7.62–7.55 (m, 2H), 7.09 (s, 2H), 6.70 (m, $J$ = 17.0, 10.2 Hz, 1H), 6.34 (d, $J$ = 16.8 Hz, 1H), 5.81 (d, $J$ = 10.1 Hz, 1H), 2.23 (s, 6H). $^{13}$C NMR (101 MHz, DMSO) $\delta$ 164.24, 155.18, 153.47, 152.06, 141.90, 139.57, 136.03, 135.66, 132.14, 131.58, 128.20, 127.59, 127.03, 126.50, 119.92, 118.13, 115.54, 112.16, 18.74.

*4.1.3. General procedure for the synthesis of quinazolinone cyclobutanebiamide derivatives 18a-18g*

*4.1.3.1. 7-(4-aminophenyl)quinazolin-4(3H)-one (13).* A flask charged with $Pd(PPh_3)_4$ (1.27 g, 1.10 mmol), potassium carbonate (4.55 g, 33.00 mmol), 4-aminobenzene boronic acid hydrochloride **3** (1.90 g, 11.00 mmol) and the key intermediate **12** (2.50 g, 11.00 mmol) were flushed with nitrogen and suspended in 1,4-dioxane (120 mL) and water (40 mL). The mixture was then refluxed overnight under nitrogen. The hot suspension was filtered and the filtrate distilled by rotary evaporation to remove 1,4-dioxane. Water (50 mL) was added and the product was extracted with AcOEt (30 mL × 3), washed with water, and dried over $Na_2SO_4$. After filtration and concentration *in vacuo*, the residue was purified by silica gel flash chromatography (PE/AcOEt = 3:1) affording **13** as yellow solid (4.32 g, 82.92%). mp: >300 °C.

*4.1.3.2. 1-((3-fluorophenyl)carbamoyl)cyclobutene carboxylic acid (15).* 1,1-Cyclobutanedicarboxylic acid **14** (1.00 g, 6.94 mmol) was dissolved in anhydrous THF (20 mL). Then triethanolamine (1.00 mL, 6.94 mmol) was added onto the mixture and the mixture was stirred on the ice-bath for 30 min. $SOCl_2$ (0.50 mL, 6.94 mmol) was then added onto the mixture. Stirring was continued for 2h, a solution of 3-fluorobenzenamine (0.77 g, 6.94 mmol) in anhydrous THF (10 mL) was added and continued stirring for 2h. Subsequently, the ice bath was removed, and the mixture was reacted at room temperature overnight. After the completion of the reaction, the mixture was filtered and concentrated *in vacuo*, the residue was purified by silica gel flash chromatography (PE/AcOEt = 5:1) yielding **15** as white solid (0.51 g, 30.91%).

*4.1.3.3. N-(3-fluorophenyl)-N-(4-(4-oxo-3,4-dihydroquinazolin-7-yl) phenyl)cyclobutane-1,1-dicarboxamide (18a).* To a mixture of the key intermediates **13** (0.13 g, 0.53 mmol) and **15** (0.19 g, 0.80 mmol) dissolved in 5 mL of THF in ice-bath, HATU (0.36 mg, 0.95 mmol) was added. After stirring for 30 min, triethanolamine (0.07 mL, 0.53 mmol) was dropped. The reaction was warmed to the room temperature and stirred overnight. After the completion of the reaction, the mixture was filtered and the filtrate distilled by rotary evaporation to remove THF. Water (50 mL) was added and the product was extracted with AcOEt (30 mL × 3), washed with water, and dried over $Na_2SO_4$. After filtration and concentration *in vacuo*, the residue was purified by silica gel flash chromatography (PE/AcOEt = 3:1) affording as **18a** as white solid (0.18 g, yield 75.0%), HRMS $m/z$ calcd for $C_{26}H_{21}FN_4O_3$ ($[M+H]^+$) 457.1598, found 457.1631. m.p. >300 °C, $^1$H NMR (400 MHz, DMSO) $\delta$ 9.87 (s, 1H), 9.83 (s, 1H), 8.16 (d, $J$ = 8.3 Hz, 1H), 8.14 (s, 1H), 7.91 (d, $J$ = 1.3 Hz, 1H), 7.87 (s, 1H), 7.84 (s, 2H), 7.80 (d, $J$ = 8.8 Hz, 2H), 7.73–7.66 (m, 1H), 7.48 (d, $J$ = 8.4 Hz, 1H), 7.34 (m, $J$ = 15.2, 8.1 Hz, 1H), 6.90 (m, $J$ = 8.5, 2.4 Hz, 1H), 2.69 (t, $J$ = 7.9 Hz, 4H), 1.92–1.81 (m, 2H). $^{13}$C NMR (101 MHz, DMSO) $\delta$ 170.69, 170.42, 161.26, 161.03, 149.67, 146.35, 145.78, 141.31, 140.01, 133.97, 130.60, 127.87, 127.03, 125.44, 124.43, 121.59, 120.90, 116.17, 110.56, 110.35, 107.32, 107.05, 56.99, 29.77, 15.83.

The title compounds **18b-a8g** were prepared from the key intermediate **13** and **15** with a similar procedure as described for compound **18a**.

*4.1.3.4. N-(3-ethynylphenyl)-N-(4-(4-oxo-3,4-dihydroquinazolin-7-yl)phenyl)cyclobutane-1,1-dicarboxamide (18b).* White solid (yield 22.8%), HRMS $m/z$ calcd for $C_{28}H_{22}N_4O_3$ ($[M+H]^+$) 463.1692, found 463.1734. m.p. >300 °C, $^1$H NMR (400 MHz, DMSO) $\delta$ 12.26 (s, 1H), 9.81 (s, 1H), 9.77 (s, 1H), 8.16 (d, $J$ = 8.3 Hz, 1H), 8.13 (d, $J$ = 3.0 Hz, 1H), 7.90 (d, $J$ = 8.8 Hz, 2H), 7.85 (d, $J$ = 8.7 Hz, 2H), 7.80 (d, $J$ = 8.8 Hz, 2H), 7.70 (d, $J$ = 8.2 Hz, 1H), 7.33 (t, $J$ = 7.9 Hz, 1H), 7.18 (d, $J$ = 7.6 Hz, 1H), 4.19 (s, 1H), 2.69 (t, $J$ = 7.8 Hz, 4H), 1.93–1.80 (m, 2H). $^{13}$C NMR (101 MHz, DMSO) $\delta$ 170.64, 170.47, 161.01, 149.82, 146.28, 145.77, 140.01, 139.67, 133.97, 129.51, 127.87, 127.25, 127.01, 125.42, 124.54, 123.43, 122.32, 121.62, 121.13, 120.90, 83.80, 81.03, 56.93, 29.78, 15.83.

*4.1.3.5. N-(4-chloro-3-(trifluoromethyl)phenyl)-N-(4-(4-oxo-3,4-dihydroquinazolin-7-yl)phenyl)cyclobutane-1,1-dicarboxamide (18c).* White solid (yield 18.8%), HRMS $m/z$ calcd for $C_{27}H_{20}ClF_3N_4O_3$ ($[M+H]^+$) 541.1176, found 541.1209. m.p. >300 °C, $^1$H NMR (400 MHz, DMSO) $\delta$ 12.27 (s, 1H), 10.32 (s, 1H), 10.00 (s, 1H), 8.34 (s, 1H), 8.16 (d, $J$ = 8.3 Hz, 1H), 8.13 (s, 1H), 8.05 (d, $J$ = 8.2 Hz, 1H), 7.90

(s, 1H), 7.88 (d, $J$ = 8.5 Hz, 2H), 7.83 (d, $J$ = 11.0 Hz, 2H), 7.79 (s, 1H), 7.67 (d, $J$ = 8.7 Hz, 1H), 2.68 (d, $J$ = 7.1 Hz, 4H), 1.95–1.77 (m, 2H). $^{13}$C NMR (101 MHz, DMSO) $\delta$ 171.08, 170.21, 161.02, 149.81, 146.29, 145.76, 140.06, 139.09, 133.98, 132.39, 132.29, 127.85, 127.16, 127.01, 126.86, 125.40, 125.13, 124.58, 124.54, 121.61, 120.94, 119.23, 119.17, 56.99, 29.69, 15.83.

*4.1.3.6. N-(4-(4-oxo-3,4-dihydroquinazolin-7-yl)phenyl)-N-(3-(trifluoromethyl)phenyl)cyclobutane-1,1-dicarboxamide (18d).* White solid (yield 20.3%), HRMS $m/z$ calcd for $C_{27}H_{21}F_3N_4O_3$ ([M+H]$^+$) 507.1566, found 507.1600. m.p. >300 °C, $^1$H NMR (400 MHz, DMSO) $\delta$ 12.30 (s, 1H), 10.40 (s, 1H), 10.19 (s, 1H), 8.25 (s, 1H), 8.16 (d, $J$ = 8.3 Hz, 1H), 8.13 (s, 1H), 8.02 (d, $J$ = 8.2 Hz, 1H), 7.92 (s, 1H), 7.90 (d, $J$ = 1.3 Hz, 2H), 7.82 (d, $J$ = 10.1 Hz, 2H), 7.79 (s, 1H), 7.55 (t, $J$ = 8.0 Hz, 1H), 7.41 (d, $J$ = 7.7 Hz, 1H), 2.69 (t, $J$ = 7.8 Hz, 4H), 1.93–1.76 (m, 2H). $^{13}$C NMR (101 MHz, DMSO) $\delta$ 170.96, 170.36, 161.06, 146.32, 145.78, 140.41, 140.15, 133.94, 130.24, 129.59, 127.85, 127.01, 125.97, 125.40, 124.51, 123.96, 123.26, 121.60, 120.90, 120.22, 116.59, 57.05, 29.81, 15.77.

*4.1.3.7. N-(3,5-bis(trifluoromethyl)phenyl)-N-(4-(4-oxo-3,4-dihydroquinazolin-7-yl)phenyl)cyclobutane-1,1-dicarboxamide (18e).* White solid (yield 23.2%), HRMS $m/z$ calcd for $C_{28}H_{20}F_6N_4O_3$ ([M+H]$^+$) 575.1440, found 575.1471. m.p. >300 °C, $^1$H NMR (400 MHz, DMSO) $\delta$ 12.30 (s, 1H), 11.03 (s, 1H), 10.38 (s, 1H), 8.57 (s, 2H), 8.16 (d, $J$ = 8.3 Hz, 1H), 8.13 (s, 1H), 7.95 (s, 1H), 7.92 (d, $J$ = 12.1 Hz, 2H), 7.82 (d, $J$ = 12.8 Hz, 2H), 7.77 (d, $J$ = 9.4 Hz, 2H), 2.74 (t, $J$ = 7.5 Hz, 4H), 1.94–1.78 (m, 2H). $^{13}$C NMR (101 MHz, DMSO) $\delta$ 170.96, 170.36, 161.06, 146.32, 145.78, 140.41, 140.15, 133.94, 130.24, 129.59, 127.85, 127.01, 125.97, 125.40, 124.51, 123.96, 123.26, 121.60, 120.90, 120.22, 116.59, 57.05, 29.81, 15.77.

*4.1.3.8. N-(3-chloro-4-methylphenyl)-N-(4-(4-oxo-3,4-dihydroquinazolin-7-yl)phenyl)cyclobutane-1,1-dicarboxamide (18f).* White solid (yield 22.3%), HRMS $m/z$ calcd for $C_{27}H_{23}ClN_4O_3$ ([M+H]$^+$) 487.1459, found 487.1498. m.p. >300 °C, $^1$H NMR (400 MHz, DMSO) $\delta$ 12.26 (s, 1H), 9.83 (s, 1H), 9.80 (s, 1H), 8.16 (d, $J$ = 8.3 Hz, 1H), 8.13 (s, 1H), 7.89 (d, $J$ = 9.6 Hz, 2H), 7.86 (d, $J$ = 8.9 Hz, 2H), 7.81 (s, 2H), 7.79 (s, 1H), 7.52 (d, $J$ = 7.9 Hz, 1H), 7.27 (d, $J$ = 8.2 Hz, 1H), 2.68 (t, $J$ = 7.3 Hz, 4H), 2.27 (s, 3H), 1.94–1.74 (m, 2H). $^{13}$C NMR (101 MHz, DMSO) $\delta$ 170.54, 170.46, 161.02, 149.80, 146.29, 145.77, 140.03, 138.62, 133.95, 133.27, 131.45, 130.62, 127.86, 127.01, 125.41, 124.53, 121.61, 120.88, 120.50, 119.12, 56.90, 29.78, 19.40, 15.82.

*4.1.3.9. N-(4-bromo-2-methylphenyl)-N-(4-(4-oxo-3,4-dihydroquinazolin-7-yl)phenyl)cyclobutane-1,1-dicarboxamide (18g).* White solid (yield 20.2%), HRMS $m/z$ calcd for $C_{27}H_{23}BrN_4O_3$ ([M+H]$^+$) 531.0954, found 531.0988. m.p. >300 °C, $^1$H NMR (400 MHz, DMSO) $\delta$ 12.26 (s, 1H), 9.85 (s, 1H), 9.22 (s, 1H), 8.17 (d, $J$ = 8.3 Hz, 1H), 8.14 (s, 1H), 7.92 (s, 1H), 7.87 (d, $J$ = 8.8 Hz, 3H), 7.82 (d, $J$ = 8.9 Hz, 2H), 7.43 (s, 1H), 7.37 (m, $J$ = 8.5, 1.7 Hz, 1H), 7.30 (d, $J$ = 8.5 Hz, 1H), 2.77–2.66 (m, 2H), 2.14 (s, 1H), 1.88 (m, $J$ = 15.0, 7.4 Hz, 2H). $^{13}$C NMR (101 MHz, DMSO) $\delta$ 171.03, 170.35, 161.04, 149.81, 146.30, 145.78, 139.97, 136.25, 136.03, 134.02, 133.12, 129.27, 128.35, 127.89, 127.02, 125.43, 124.56, 121.63, 120.97, 118.47, 56.27, 29.71, 17.67, 15.91.

### 4.2. In vitro angiogenic RTKs inhibition assays [23]

The *in vitro* kinase inhibition assays against VEGFR-2, TIE-2, and EphB4 of all the title compounds were detected using the ADP-Glo™ kinase assay kit (Promega, Madison) with sorafenib as positive control. The kinase assay was performed in duplicate in a reaction mixture of final volume of 10 μL. General procedures are as the following: for VEGFR-2 assays, the tyrosine kinase (0.6 ng/mL) were incubated with substrates (0.2 mg/mL), tested title compounds ($1.2 \times 10^{-4}$~12 μM) and ATP (50 μM) in a final buffer of Tris 40 mM, $MgCl_2$ 10 mM, BSA 0.1 mg/mL, DTT 1 mM in 384-well plate with the total volume of 5 μL. The assay plate was incubated at 30 °C for 1 h. After the plate was cooled at r.m. for 5 min, 5 μL of ADP-Glo reagent was added into each well to stop the reaction and consume the remaining ADP within 40 min. At the end, 10 μL of kinase detection reagent was added into the well and incubated for 30 min to produce a luminescence signal. As for TIE-2 and EphB4 assays, the tyrosine kinase (2.4 ng/mL)were incubated with substrates (0.2 mg/mL), tested title compounds ($1.2 \times 10^{-4}$~12 μM) and ATP (50 μM) in a final buffer of Tris 40 mM, $MgCl_2$ 10 mM, BSA 0.1 mg/mL, DTT 1 mM in 384-well plate with the total volume of 5 μL. The assay plate was incubated at 30 °C for 4 h. After the plate was cooled at room temperature for 5 min, 5 μL of ADP-Glo reagent was added into each well to stop the reaction and consume the remaining ADP within 1 h. At the end, 10 μL of kinase detection reagent was added into the well and incubated for 30 min to produce a luminescence signal. The luminescence was read by VICTOR-X multi-label plate reader.

### 4.3. Human vascular endothelial cell (EA.hy926) viability assay [24]

The viability of HUVEC (EA.hy926) was assessed using the cell counting kit-8 (CCK-8, Sigma, USA) assay according to the manufacturer's instruction. In brief, EA-hy926 cells were harvested and plated in a 96-well plate at the density of $1 \times 10^5$ cells for each well and cultured in DMEM containing 10% FBS in humidified 5% $CO_2$ atmosphere. After incubation at 37 °C for 48 h, the cells were treated with tested compounds at various concentrations for 24 h. Subsequently, premixed CCK-8 and medium (10 μL) were added into the 96-well plates to monitor cell viability and were incubated at 37°C for 2 h. The number of viable cells was assessed by measurement of absorbance at 450 nm by a microplate reader. The viability rate was calculated as experimental OD value/control OD value.

### 4.4. Cell growth inhibitory activity in cancer cell lines [25]

The anticancer activity of the most potent compound 16a was evaluated against nine cancer cell lines by the standard MTT assay *in vitro*, with sorafenib as positive drug. Exponentially growing cells were harvested and plated in 96-well plates at a concentration of $1 \times 10^4$ cells/well per well, and then were incubated at 37 °C for 24 h. The tested compound at the indicated final concentrations were added to the culture medium and incubated for 48 h. Fresh MTT was added to each well at the terminal concentration of 0.5 mg/mL, and incubated with cells at 37 °C for 4 h. After the supernatant was discarded, 150 μL DMSO was added to each well, and the absorbance values were determined by a microplate reader (Bio-Rad, Hercules, CA, USA) at 490 nm.

### 4.5. Molecular docking modeling [26]

In order to understand the binding mode of inhibitors with VEGFR-2/TIE-2/EphB4, molecule docking was performed using Sybyl-X/Surflex-dock module based on the crystal structures of VEGFR-2 (PDB ID: 4ASD), TIE-2 (PDB ID: 2P4I) and EphB4 (PDB ID: 2X9F). Hydrogen was added and minimized using the Tripos force field and Pullman charges. The most potent compound (16a) was depicted with the Sybyl-X/Sketch module (Tripos Inc.) and optimized applying Powell's method with the Tripos force field with convergence criterion set at 0.05 kcal/(Åmol), and assigned with the Gasteiger-Hückel charge. The docking studied was carried out

using Surflex-dock module. The residues in a radius 5.0 Å around the natural ligand of VEGFR-2/TIE-2/EphB4 in the crystal complex were selected as the active site. Other docking parameters were kept at default.

## Acknowledgments

This work was supported by the National Natural Science Foundation of China (*NSFC*, Grant No. 81573285), the Natural Science Basic Research Plan in Shaanxi Province of China (Program No. 2015JQ8312), and the Fundamental Research Funds for the Central Universities (2015qngz13).

## Appendix A. Supplementary data

Supplementary data related to this article can be found at https://doi.org/10.1016/j.ejmech.2017.10.008.

## References

[1] B.R. Zetter, The scientific contributions of M. Judah Folkman to cancer research, Nat. Rev. Cancer 8 (2008) 647–654.
[2] D. Bouïs, Y. Kusumanto, C. Meijer, N.H. Mulder, G.A. Hospers, A review on pro- and anti-angiogenic factors as targets of clinical intervention, Pharmacol. Res. 53 (2006) 89–103.
[3] Z. Lin, Q. Zhang, W. Luo, Angiogenesis inhibitors as therapeutic agents in cancer: challenges and future directions, Eur. J. Pharmacol. 793 (2016) 76–81.
[4] A. Martínez, A new family of angiogenic factors, Cancer Lett. 236 (2006) 157–163.
[5] G. Martiny-Baron, P. Holzer, E. Billy, C. Schnell, J. Brueggen, M. Ferretti, N. Schmiedeberg, J.M. Wood, P. Furet, P. Imbach, The small molecule specific EphB4 kinase inhibitor NVP-BHG712 inhibits VEGF driven angiogenesis, Angiogenesis 13 (2010) 259–267.
[6] D. Hanahan, J. Folkman, Patterns and emerging mechanisms of the angiogenic switch during tumorigenesis, Cell 86 (1996) 353–364.
[7] D. Huang, H. Lan, F. Liu, S. Wang, X. Chen, K. Jin, X. Mou, Anti-angiogenesis or pro-angiogenesis for cancer treatment: focus on drug distribution, Int. J. Clin. Exp. Med. 8 (2015) 8369–8376.
[8] J.S. Papadopoulos, R. Agarwala, COBALT: constraint-based alignment tool for multiple protein sequences, Bioinformatics 23 (2007) 1073–1079.
[9] X. Robert, P. Gouet, Deciphering key features in protein structures with the new ENDscript server, Nucleic Acids Res. 42 (2014) W320–W324.
[10] J. Zhang, Y. Zhang, S. Zhang, S. Wang, L. He, Discovery of novel taspine derivatives as antiangiogenic agents, Bioorg Med. Chem. Lett. 20 (2010) 718–721.
[11] J. Zhang, Y. Zhang, Y. Shan, N. Li, W. Ma, L. He, Synthesis and preliminary biological evaluation of novel taspine derivatives as anticancer agents, Eur. J. Med. Chem. 45 (2010) 2798–2805.
[12] C. Wang, H. Gao, J. Dong, Y. Zhang, P. Su, Y. Shi, J. Zhang, Biphenyl derivatives incorporating urea unit as novel VEGFR-2 inhibitors: design, synthesis and biological evaluation, Bioorg Med. Chem. 22 (2014) 277–284.
[13] H. Gao, P. Su, Y. Shi, X. Shen, Y. Zhang, J. Dong, J. Zhang, Discovery of novel VEGFR-2 inhibitors. Part II: biphenyl urea incorporated with salicylaldoxime, Eur. J. Med. Chem. 90 (2015) 232–240.
[14] W. Lu, P. Li, Y. Shan, P. Su, J. Wang, Y. Shi, J. Zhang, Discovery of biphenyl-based VEGFR-2 inhibitors. Part 3: design, synthesis and 3D-QSAR studies, Bioorg Med. Chem. 23 (2015) 1044–1054.
[15] P. Su, J. Wang, Y. Shi, X. Pan, R. Shao, J. Zhang, Discovery of biphenyl-aryl ureas as novel VEGFR-2 inhibitors. Part 4: exploration of diverse hinge-binding fragments, Bioorg Med. Chem. 23 (2015) 3228–3236.
[16] Y. Shan, H. Gao, X. Shao, J. Wang, X. Pan, J. Zhang, Discovery of novel VEGFR-2 inhibitors. Part 5: exploration of diverse hinge-binding fragments via core-refining approach, Eur. J. Med. Chem. 103 (2015) 80–90.
[17] B. Dai, J. Qi, R. Liu, J. Zhang, Y. Zhan, Y. Zhang, A novel compound T7 (N-{4'-[(1E)-N-hydroxyethanimi doyl]-3',5,6-trimethoxybiphenyl-3-yl}-N'-[4-(3-morph olin-4-ylpropoxy)phenyl]urea) screened by tissue angiogenesis model and its activity evaluation on anti-angiogenesis, Phytomedicine 21 (2014) 1675–1683.
[18] X. Pan, F. Wang, Y. Zhang, H. Gao, Z. Hu, S. Wang, J. Zhang, Design, synthesis and biological activities of Nilotinib derivates as antitumor agents, Bioorg Med. Chem. 21 (2013) 2527–2534.
[19] S. Ravez, A. Barczyk, P. Six, A. Cagnon, A. Garofalo, L. Goossens, P. Depreux, Inhibition of tumor cell growth and angiogenesis by 7-aminoalkoxy-4-aryloxy-quinazoline ureas, a novel series of multi-tyrosine kinase inhibitors, Eur. J. Med. Chem. 79 (2014) 369–381.
[20] B. Daydé-Cazals, B. Fauvel, M. Singer, C. Feneyrolles, B. Bestgen, F. Gassiot, A. Spenlinhauer, P. Warnault, N. Van Hijfte, N. Borjini, G. Chevé, A. Yasri, Rational design, synthesis, and biological evaluation of 7-azaindole derivatives as potent focused multi-targeted kinase inhibitors, J. Med. Chem. 59 (2016) 3886–3905.
[21] J. Wang, L. Zhang, X. Pan, B. Dai, Y. Sun, C. Li, J. Zhang, Discovery of multi-target receptor tyrosine kinase inhibitors as novel anti-angiogenesis agents, Sci. Rep. 7 (2017) 45145.
[22] S. Wang, J. Chen, Y. Fu, X. Chen, Promotion of astragaloside IV for EA-hy926 cell proliferation and angiogenic activity via ERK1/2 pathway, J. Nanosci. Nanotechnol. 15 (2015) 4239–4244.
[23] Y.H. Peng, H.Y. Shiao, C.H. Tu, P.M. Liu, J.T. Hsu, P.K. Amancha, J.S. Wu, M.S. Coumar, C.H. Chen, S.Y. Wang, W.H. Lin, H.Y. Sun, Y.S. Chao, P.C. Lyu, H.P. Hsieh, S.Y. Wu, Protein kinase inhibitor design by targeting the Asp-Phe-Gly (DFG) motif: the role of the DFG motif in the design of epidermal growth factor receptor inhibitors, J. Med. Chem. 56 (2013) 3889–3903.
[24] H.B. Shi, J.D. Chen, X.H. Chen, Y. He, Z.J. Yang, Effects of salvianolic acid and notoginseng triterpenes on angiogenesis in EA-hy926 cells in vitro, Chin. J. Nat. Med. 11 (2013) 254–257.
[25] L. Zhang, Y. Shan, C. Li, Y. Sun, P. Su, J. Wang, L. Li, X. Pan, J. Zhang, Discovery of novel anti-angiogenesis agents. Part 6: multi-targeted RTK inhibitors, Eur. J. Med. Chem. 127 (2017) 275–285.
[26] J. Zhang, Y. Shan, X. Pan, C. Wang, W. Xu, L. He, Molecular docking, 3D-QSAR studies, and in silico ADME prediction of p-aminosalicylic acid derivatives as neuraminidase inhibitors, Chem. Biol. Drug Des. 78 (2011) 709–717.